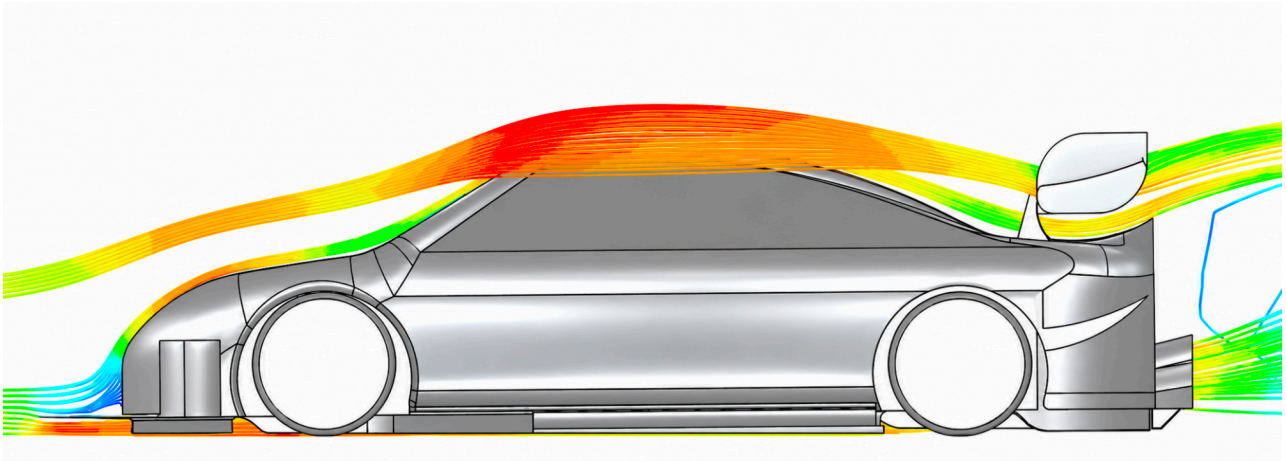
Parametric Investigation of Aerodynamic Performance in a GT-Style Race Car

---

A Progressive Study of Race Car Aerodynamic Devices Using Computational Fluid Dynamics

---



Arjuna Sankar
Mayoor Private School,
Abu Dhabi
July 2026
Independent Research Project

1. Abstract

Most race car aerodynamic packages are developed iteratively, although the interaction between progressively added aerodynamic devices remains an important area of study. This study investigates the aerodynamic evolution of a simplified GT-style race car using RANS CFD with the k-ω SST turbulence model at 200 km/h. Eight configurations (A-H) were analyzed, gradually introducing components like a ducktail spoiler, rear wing, and more. The baseline design featured a drag coefficient of 0.304 and a positive lift coefficient of +0.476. Subsequent iterations resulted in configuration H achieving a lift coefficient of -1.452 and a 405% shift in lift coefficient compared to the baseline with a drag coefficient of 0.573. Various non-linear interaction effects were identified, indicating that effective aerodynamic development requires a holistic system approach rather than simply adding components. However no diminishing returns were observed in the performance metrics across configurations.

2. Nomenclature

Symbol / Acronym	Definition
Cd	Coefficient of Drag
Cl	Coefficient of Lift
Cl(f)	Front Lift Coefficient
Cl(r)	Rear Lift Coefficient
Cm	Moment Coefficient
Cp	Pressure Coefficient
Re	Reynolds Number
ρ	Air Density
V∞	Freestream Velocity
A	Reference Frontal Area
μ	Dynamic Viscosity
p	Static Pressure
p∞	Freestream Static Pressure
F(D)	Drag Force
F(L)	Lift Force
L/D	Lift-to-Drag Ratio
ω	Specific Dissipation Rate
RANS	Reynolds-Averaged Navier–Stokes
SST	Shear Stress Transport
K-ω SST	K-omega Shear Stress Transport (turbulence model)
CFD	Computational Fluid Dynamics
CAD	Computer-Aided Design
AoA	Angle of Attack

3. Introduction

High-speed racing vehicles' efficiency and performance are largely determined by vehicle aerodynamics. Aerodynamic forces tend to rapidly equal or exceed the mechanical grip as vehicle speed increases, having a direct impact on the tire loading, cornering ability, and lap times of race cars. Such cars intentionally produce aerodynamic downforce to improve tire grip and vehicle stability during high-speed maneuvers, in contrast to road vehicles, where the primary objective of aerodynamic development largely is on decreasing drag to improve fuel economy. Greater lateral acceleration and better handling performance are made possible with this added vertical load given by downforce, but aerodynamic drag and the power needed to sustain high speeds are unavoidably increased. Consequently, the aerodynamic design of race cars is essentially at heart an optimization problem where the advances in downforce must be weighed against the corresponding drag penalty associated with the production of it. This trade-off has been the crux of substantial scholarly and commercial research and is still one of the primary issues in motorsports aerodynamics.

Downforce is primarily produced by the manipulation of pressure fields along the surface of aerodynamic elements around a race car. According to fluid dynamic principles, accelerating airflow around aerodynamic surfaces decreases the local static pressure around it, these pressure differentials create a net force directed towards the ground. Devices commonly found in GT race cars such as Rear wings, Diffusers, front splitters, canards, and other bodywork, exploit these principles by controlling airflow to maximise these pressure differentials and subsequently producing downforce while minimizing flow separation and other aerodynamic losses. However, as aerodynamic loading increases, adverse pressure gradients get stronger, increasing the likelihood of flow separation, wake growth, and pressure drag. This resulting complex interaction between aerodynamic elements means that the improvements and downforce of one element cannot be studied independently without looking at the effect and influence it has on other elements of the car, as elements in the front of the car greatly sway the flow structure and performance of subsequent elements downstream, a phenomenon known as Aerodynamic interference or Upwash-Downwash coupling. As a result, the aerodynamic performance of a singular part is not merely a result of its geometry but also the interaction it has with the wider flow field around the vehicle.

Advances in Computational Fluid Dynamics(CFD) have transformed the broader aerodynamic research and design field by allowing engineers and researchers to evaluate multiple differing design choices before physical prototyping and wind tunnel testing. Modern Reynolds-Averaged Navier–Stokes (RANS) solvers,along with turbulence models such as Shear Stress Transport ($k-\omega$ SST) models have allowed a good practical balance between computational cost and research value given by its predictive nature of external airflow involving flow separation, pressure gradients and wake structures around vehicles. Even though Large Eddy Simulation (LES) and other higher-fidelity methods provide better transient flow prediction, their computational requirements remain impractical for large parametric studies such as this. Therefore Steady-State RANS simulations form the backbone of modern industry and academic research.

Numerous papers have dealt with the examination of both individual aerodynamic parts and development of overall racing aerodynamics packages using an iterative process. Some examples of such analysis include parametric studies of the additional devices added to DrivAer race cars[1] and sequential CFD optimization of the entire Formula Student aerodynamics package[2]. The presented study, on the other hand, focuses on following the evolutionary process of one simple GT vehicle using a specific configuration sequence, paying special attention to interaction effects that occur due to the addition of individual devices. This approach allows for the study of the performance of a

single element along with the positive or negative impact and interaction with other elements present. It also provides greater insight at the point greater aerodynamic complexity yields diminishing results in the downforce and the aerodynamic efficiency of the vehicle
Accordingly, this study presents a parametric investigation of differing aerodynamic elements based on a simplified GT car model similar to the DrivAER model of the Technical University of Munich, a simplified base car body which amplifies the addition of aerodynamic devices. Eight progressively developed configurations were tested in an identical simulation environment. This investigation evaluates the evolution of Drag coefficient (Cd), Lift coefficient (Cl), Moment Coefficient (Cm) along with the pressure distribution, flow structure and general aerodynamic balance of the car. An additional emphasis is placed on identifying the aerodynamic mechanisms responsible for performance changes and whether the application of additional flow conditioners and aero devices constitutes a meaningful impact or exhibits diminishing results

4. Theoretical Background

4.1 Race Car Aerodynamics

Race car aerodynamics work by creating a pressure differential along the aerodynamic surfaces of an element to generate a net downward force at the cost of increasing the net drag of the car [3].

4.1.1 Fundamentals of Race Car Aerodynamics

4.1.1.1 Pressure Distribution

The aerodynamic behaviour of a race car is defined by the pressure distribution over its body surfaces. As air flows over the bodywork and aerodynamic elements of a race car, changes to the velocity of the air causes a change in the local static pressure (p) in accordance with Bernoulli's principle. Regions where the airflow accelerates experience a decrease in local static pressure (p) while regions where airflow stagnates or slows down experience an increase in local static pressure (p). [3][4]

4.1.1.2 Downforce

The net aerodynamic force acting downwards on a vehicle is called downforce. It increases the normal force on the wheels without increasing the mass of the car. Since tyre grip is proportional to the normal force given by.

$$N = mg + F_{(downforce)} \qquad Eqn.(1)$$

Where downforce is given by

$$F_l = \frac{1}{2}\rho V^2 A C_l \qquad Eqn.(2)$$

And the maximum tyre grip is given by.

$$F_{(friction,max)} = \mu_{(tyre)} N_{(normal)} \qquad Eqn.(3)$$

Increasing downforce enables greater cornering speeds and vehicle stability; consequently, modern racing vehicles rely heavily on aerodynamic downforce to increase performance and enhance their lap times. [3][5]

4.1.1.3 Aerodynamic Drag

Aerodynamic drag is the resistive force experienced by the vehicle as it travels through air. It represents one of the major limiting factors regarding maximum speed and aerodynamic efficiency. It consists of Pressure drag along with Skin-Friction drag. Pressure drag arises from the pressure differential between the front of the car and the rear of the car due to flow seperation, while Skin-Friction drag results from the viscous shear stresses acting along the boundary layer of the vehicle surface. [4][5]

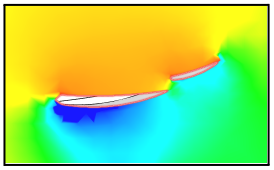
The aerodynamic drag force acting on a vehicle travelling through a freestream is given by

$$F_d = \frac{1}{2}\rho V^2 A C_d \qquad Eqn.(4)$$

4.1.1.4 Boundary Layer

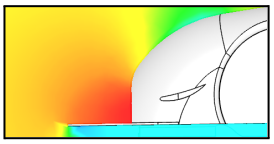
The boundary layer consists of the thin layer of fluid immediately adjacent and tangent to the surface of the vehicle. Airflow velocity is zero at the vehicle surface and slowly increases to freestream velocity as we travel further away from the vehicle surface. The behaviour strongly influences whether airflow stays attached to an aerodynamic surface. [5][6]

4.1.2 Rear Wing



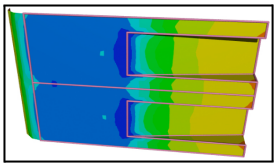
Wings on a race car act as inverted aerofoils, it accelerates airflow flowing beneath the wing and decelerate airflow flowing above it. This in accordance to Bernoulli's principle, causes a low-pressure suction region below the wing and a high-pressure region above it. This is the most direct and tunable Aerodynamic device on a race car; however, it brings along the highest drag penalty in the form of high induced drag along with vortex and wake losses. This is demonstrated in Fig. 4.1.2. [3]

4.1.3 Splitter



A splitter works by creating a high-pressure stagnation zone above the splitter plane while allowing fast-moving, low-pressure air to flow below the splitter plane. It has a comparatively low drag penalty. This is demonstrated in Fig 4.1.3. [3][5]

4.1.4 Diffuser



Diffusers recover pressure at the rear end of the car by slowly increasing the pressure of the fast-moving, low-pressure air at the underbody of the car by gradually expanding the flow area. It allows the underbody to run at a much lower pressure for a greater length while controlling flow separation at the rear of the vehicle. This is demonstrated in Fig 4.1.4. [3]

4.2 Computational Fluid Dynamics in Motorsports.

Computational Fluid Dynamics(CFD) has become an indispensable tool in modern motorsports by allowing engineers and researchers to evaluate the aerodynamic performance of the car and is used in place of, or alongside, physical wind tunnel testing. It provides detailed information on the pressure differential, wake, velocity streamlines and boundary layer behavior of the car allowing for rapid prototyping and iterative optimisation. [1]

4.3 Turbulence Model Selection: k-ω SST vs k-ε

Both turbulence model: k-ω SST and k-ε constitute two equation RANS models, however, they are optimized for two different regions of airflow

4.3.1 k-ε

K-ε is a robust and computationally cheap model which works strong in fully turbulent flow far away from walls, however it is known to underperform when it interacts with adverse pressure gradients which are present in diffuser ramps and wing suction surfaces in near stall conditions [7]

4.3.2 k-ω SST

k-ω SST blends the K-ε model in the freestream air along with the k-ω model(which resolves viscous flow near walls exceptionally) near the wall using a blending functions. According to SimScale's documentation, this hybrid formulation is specifically what makes k-ω SST reliable for separation prediction, since standard k-ω alone is over-sensitive to freestream turbulence values, and standard k-ε alone is unreliable near adverse pressure gradients. [6][7]

4.3.3 Final Decision

Given that this study's primary objective is to evaluate the aerodynamic performance and efficiency of the car as progressively complex downforce-generating and flow conditioning aerodynamic elements are added to the vehicle, the choice of the CFD model was exceptionally important. These devices and elements are operating in high adverse pressure gradients, where accurate prediction of boundary layer flow and flow separation are critically important. Consequently the k-ω SST model was chosen because of its superior ability to predict near wall flow and blend the accuracy of K-ε in free stream flow making it the appropriate model to be used in this study.

Characteristic	Standard k-ε	Standard k-ω	k-ω SST
Primary application	Free stream flow	Near-wall flow	Used for both
Near-wall accuracy	Moderate	Excellent	Excellent
Free-stream sensitivity	Low	High	Low (through blending)
Adverse pressure gradients	Moderate	Good	Excellent
Flow separation prediction	Limited	Good	Excellent
Boundary-layer modelling	Moderate	Excellent	Excellent

(Table 4.3) Comparison between k-ε, k-ω and k-ω SST.

5. Research Design

5.1 Research Aim

This investigation aims to evaluate the influence of progressively introduced aerodynamic devices on the performance of a simplified GT-style sports car using Computational Fluid Dynamics (CFD). Specifically, the study seeks to:

A. Quantify the individual and cumulative overarching effects of aerodynamic devices, including a ducktail spoiler, rear wing, front splitter, diffuser, side skirts, and variable-height underbody on drag coefficient (Cd) and lift coefficient (Cl) across a progressive configuration matrix (A–H).
B. Characterize the interaction effects between front and rear aerodynamic elements, examining how upstream devices alter the flow field encountered by downstream components.
C. Identify regions of flow separation, wake formation, and pressure recovery within each configuration and to assess the physical mechanisms underlying observed force coefficient trends.
D. Determine the configuration, or range of configurations, that represents the most efficient trade-off between downforce generation and aerodynamic drag, using the Cd–Cl relationship across the full parametric matrix to identify points of diminishing aerodynamic return.

5.2 Research Questions

The investigation seeks to answer the following research questions:

A. How much aerodynamic benefit does each individual aerodynamic device contribute to the overall package?
B. Do combinations of aerodynamic devices produce additive, synergistic, or diminishing aerodynamic performance gains?

C. At what stage does increasing aerodynamic complexity result in a disproportionately large drag penalty?
D. How do successive aerodynamic modifications influence pressure distribution, flow attachment, boundary-layer separation, and wake development?
E. Which configuration provides the optimum balance between downforce generation and aerodynamic efficiency?

5.3 Progressive Aerodynamic Configuration Matrix

Configuration	Devices Added	Description
A	None (clean baseline body)	Clean reference case with no aerodynamic devices, establishes baseline lift/drag.
B	Ducktail Spoiler	Isolates rear body pressure recovery effect of a ducktail spoiler
C	Simple Rear Wing	Isolates Lift/Drag of a single element simple wing independent of a spoiler
D	Simple Rear Wing + Ducktail Spoiler	Combines Lift/Drag of a single element simple wing along with a spoiler to study whether their effects are additive or subtractive
E	Simple Rear wing + Ducktail Spoiler + Front Splitter	Introduces Front splitter to Introduce the concept of Aero balance and Upwash/Downwash Coupling.
F	Simple Rear wing + Ducktail Spoiler + Front Splitter + Simple Diffuser	Addition of a Simple diffuser to experiment with underbody pressure recovery
G	Complex Rear wing + Ducktail Spoiler + Front Splitter + Simple Diffuser + Side Skirts	Upgrades to a complex multi element Rear wing along with endplate canards and also introduces Side skirts along the floor to seal the underbody and prevent lateral leakage.
H	Complex Rear wing + Ducktail Spoiler + Front Splitter + Variable Height Diffuser + Side Skirts + Flow Conditioners	Adds flow conditioners to reduce the influence of front and rear wheel wake on diffuser extraction and to reduce pressure drag.

Table (5.3) Progressive Configuration Matrix.

The configuration matrix presented in table(5.3) outlines the systematic development sequence adopted throughout this study. Rather than compare unrelated individual vehicle configurations which do not have a real world usage, each successive configuration introduces a related singular aerodynamic device or a logically related group of devices while maintaining an identical unchanged baseline vehicle. This prioritises not only the individual aerodynamic effect but also how each element further influences other aerodynamic surfaces around the vehicle under consistent simulation conditions. While each component can be studied individually, the combined behaviour is often non-linear due to changes in pressure distribution, wake development and vortex formation. This resulting framework provides a structured basis for evaluating such configurations.

5.4 Overarching Hypothesis

It is to be hypothesised that the progressive addition of aerodynamic devices will initially produce improvements in downforce generation and the management of aerodynamic drag through greatly enhanced pressure distribution and underbody flow management. However, beyond a certain point of aerodynamic complexity, the incremental increase in downforce is expected to diminish while the aerodynamic drag increases at a disproportionately greater rate. Consequently, an intermediate configuration is predicted to provide the most favourable compromise between downforce generation and drag, rather than the most aerodynamically complex configuration.

6.Computational Methodology

6.1 CAD design

6.1.1 Design Inspiration

The baseline body used in this study was inspired by the idea of the *DrivAer* reference model developed by the Technical University of Munich (TUM) [8][9]. The DrivAer model was designed as an open source benchmark geometry that consists of the essential aerodynamic features of a commercial production vehicle while simplifying geometry. Adopting a similarly simplified GT-style geometry allowed the aerodynamic contribution of each progressively added device to be isolated and studied without the interference from highly detailed production features which are not essential to our objective. The model also followed the philosophy of a lightweight and relatively compact sports focused car and has taken up the proportions as such.
A highly detailed GT3 race car was intentionally not used as the baseline geometry for this study, as integrated aerodynamic features present on production race cars would make it much more difficult to isolate the individual contribution of each aerodynamic element introduced during the parametric investigation.

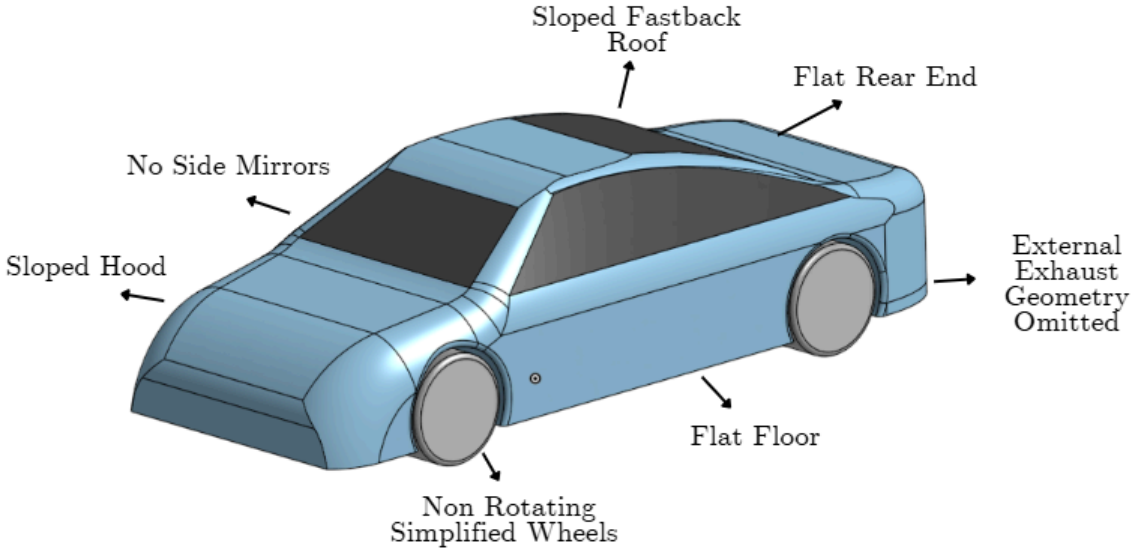
6.1.2 Design Simplification

Simplification	Reason
Mirrors removed	Reduce geometric complexity and meshing effort; negligible effect on study objectives.
Cooling ducts omitted	Internal cooling flow not investigated.
Exhaust removed	No influence on external aerodynamics considered.
Simplified wheels	Focus on body aerodynamics rather than detailed wheel flow.
No wheel rotation	Reduces computational cost; consistent across all configurations.
Flat Floor	Provides a controlled baseline for diffuser development

(Table 6.1.2) Overview on omitted parts from the baseline geometry.

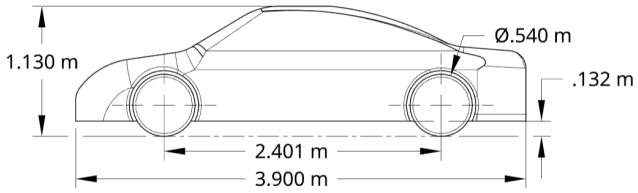
All simulations are equally impacted by the simplifications as all configurations employ the same baseline geometry. Therefore, the relative changes between configurations are valid for comparative analysis even when the absolute aerodynamic coefficients may be different from those of a production GT car.

6.1.3 Baseline Cad Geometry

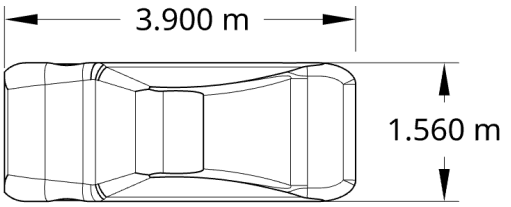


(Figure 6.1.3(a)) Baseline GT-style CAD model showing the principal geometric features and simplifications adopted for the present investigation.

Figure 6.1.3(a) illustrates the simplified baseline geometry used throughout the investigation. In order to save mesh complexity and computational expense, a number of external features, such as side mirrors, exhaust ports, and intricate wheel shapes, were purposely left out. Because of these simplifications, it is possible to assess the impact of the progressively introduced aerodynamic devices with little interference from secondary flow structures while keeping the baseline geometry constant for all configurations.



(Figure 6.1.3(b)) Side view & Dimensions.



(Figure 6.1.3(c)) Top view & Dimensions.

The primary dimensions of the simplified baseline GT-style car used for the study are shown in Figure 6.1.3(b) along with figure 6.1.3(c). Compact sports car proportions were maintained in the model's development, but the external shape was kept simple enough for CFD analysis. These dimensions were selected to represent a realistic lightweight GT platform, and held constant across all configurations to isolate the effect of the aerodynamic devices being tested.

Parameter	Value
Length	3.900 m
Width	1.560 m
Height	1.130 m
Wheelbase	2.401 m
Ground Clearance	0.132 m
Wheel Diameter	0.540 m

Table(6.1.3) Baseline Specifications

6.2 Computational Domain

6.2.1 Domain Design

The vehicle was enclosed in a three dimensional computational fluid domain representing an open road external aerodynamic environment. This domain was optimised to minimize the influence of external boundary layers while maintaining a reasonable computational cost. Clearance was provided upstream, downstream and along the sides and top to ensure flow and wake development were not artificially constrained by the domain boundary.

6.2.2 Domain Dimensions

Parameter	Value	Justification
Upstream Distance	2L	Allows the flow to fully develop before reaching the vehicle
Downstream Distance	6L	Captures wake development accurately
Domain Width	5L	Minimises blockage effects
Domain Height	3L	Reduces influence of upper boundary
Ground Plane	Moving Wall	Represents realistic vehicle-road relative motion
Reference Velocity	200 km/h	Representative high-speed GT racing condition

Table(6.2.2)critical dimensions of the computational domain used in the study.

Sufficient Clearance was given across all three dimensions to ensure results were not corrupted with blockage effects. A moving ground plane was employed in all simulations to accurately simulate the relative motion between the vehicle and the ground, improving the prediction of near ground and underbody flow.

6.2.3 Boundary Conditions

Boundary	Condition
Inlet	Velocity Inlet
Outlet	Pressure Outlet
Top	Slip Wall
Side Walls	Slip Walls
Ground	Moving Wall
Vehicle Surface	No-Slip Wall

The external aerodynamic environment of the GT-style race car was simulated by applying boundary conditions. The upper and side walls were subjected to slip wall conditions to reduce interference, and a velocity profile of 200 km/h and a pressure outlet were defined on the front and rear walls respectively. To accurately simulate on-road operation conditions, a moving ground plane and non-slip vehicle surfaces were employed.

Table(6.2.3) boundary conditions used for this study.

6.2.4 Mesh Generation Settings

Parameter	Setting
Meshing Algorithm	Standard
Mesh Sizing	Automatic
Fineness Level	7
Curvature Refinement	Automatic
Automatic Boundary Layers	Enabled
Physics-Based Meshing	Disabled
Hex Element Core	Disabled
Automatic Extrusion Meshing	Disabled
Preferred CPUs	Automatic (Max. 16)
Total Cells (avg across configuration)	≈ 4.2 Million
Total Nodes	≈ 2.2 Million

Table (6.2.4(a)) summarises the mesh generation settings employed throughout the investigation

Mesh Property	Value
Total Cells(Baseline)	3.5 Million
Total Nodes	2.2 Million
Meshing Runtime	0.51 Core Hours
Mesh Status	Successful

table (6.2.4(b)) outlines the mesh statistics.

SimScale's Standard meshing algorithm was used to create the computational mesh. To capture the intricate geometry of the vehicle while preserving computational efficiency, an unstructured mesh was chosen for this specific study. Surface representation and near-wall flow resolution were improved by using automatic curvature refinement and boundary layer generation, especially in the vicinity of aerodynamic devices where precise prediction of boundary-layer behavior and flow separation is crucial for the objectives for this investigation. To maintain uniformity throughout the parametric investigation, the same meshing settings were used for each configuration.

6.2.5 Numerical Solver Settings

Parameter	Setting
Flow Model	Incompressible
Simulation Type	Steady-State
Turbulence Model	k-ω SST
Pressure–Velocity Coupling Algorithm	SIMPLE
Relaxation Type	Manual
Velocity Residual Tolerance	1×10^{-6}
Pressure Residual Tolerance	1×10^{-6}
Turbulent Kinetic Energy (k) Residual Tolerance	1×10^{-6}
Specific Dissipation Rate (ω) Residual Tolerance	1×10^{-6}
Gradient Scheme	Cell-Limited Least Squares
Pressure Gradient Scheme	Cell-Limited Least Squares
Velocity Gradient Scheme	Cell-Limited Least Squares
Momentum Divergence Scheme	Gauss Linear Upwind
Turbulence (k) Divergence Scheme	Bounded Gauss Upwind
Turbulence (ω) Divergence Scheme	Bounded Gauss Upwind
Laplacian Scheme	Gauss Linear Limited
Laplacian Limiter Coefficient	0.5

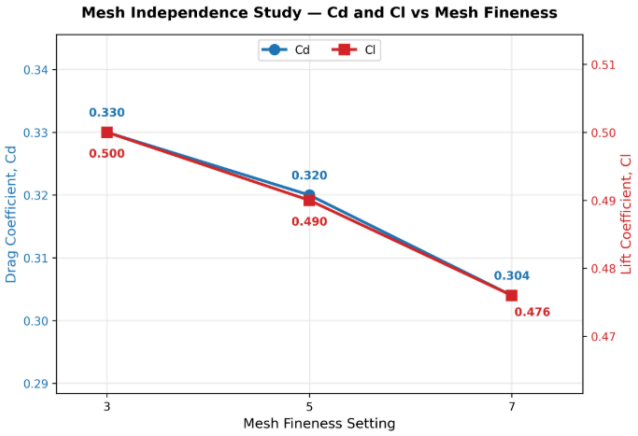
Table(6.2.5) Numerical Solver Settings

Table (6.2.5) outlines the numerical solver settings used throughout the CFD investigation. A steady-state incompressible RANS solver with the k-ω SST turbulence model was used for all simulations. The SIMPLE pressure–velocity coupling algorithm was adopted together with second-order accurate spatial discretisation schemes.

6.2.6 Mesh Sensitivity Study

Mesh setting	Cd	Cl	Cm
3 (986k cells)	0.330	0.500	-0.077
5 (1.4m cells)	0.320	0.490	-0.084
7 (3.5m cells)	0.304	0.476	-0.083

Table(6.2.6) Mesh Independence Table



The aerodynamic coefficients had convergent values when the mesh resolution increased.Cd and Cl varied by 2–5% between mesh levels 3–7; results are reported at setting 7 as the finest level computationally feasible, though full asymptotic convergence was not confirmed. The mesh level 7 was selected for conducting the parametric study because it provided maximum resolution.

6.2.7 Validation

The numerical methodology was validated through the use of a mesh sensitivity study, confirming that further mesh refinement produced almost negligible changes ; convergence monitoring of residuals and aerodynamic force coefficients, ensuring the stabilisation of aerodynamic force coefficients ; and the adoption of a turbulence model extensively validated for external automotive aerodynamics. Although experimental wind tunnel validation was beyond the scope of this investigation, identical numerical settings were maintained across all configurations to ensure that the reported aerodynamic trends represent genuine geometric effects rather than numerical inconsistencies.

6.2.8 Sources of Uncertainty

Source	Potential Influence
Simplified CAD Geometry	Absolute aerodynamic coefficients may differ from a real GT race car.
Omitted Cooling Ducts and Mirrors	Local flow structures not represented.
Simplified Non Rotating Wheel Geometry	Wheel wake interactions are simplified.
Steady-State RANS Assumption	Unsteady vortex shedding and transient flow behaviour are not captured.
Turbulence Model	k-ω SST remains a turbulence model approximation.
Mesh Resolution	Small numerical errors may remain despite mesh independence.
No Experimental Validation	Absolute results cannot be directly verified against physical testing.

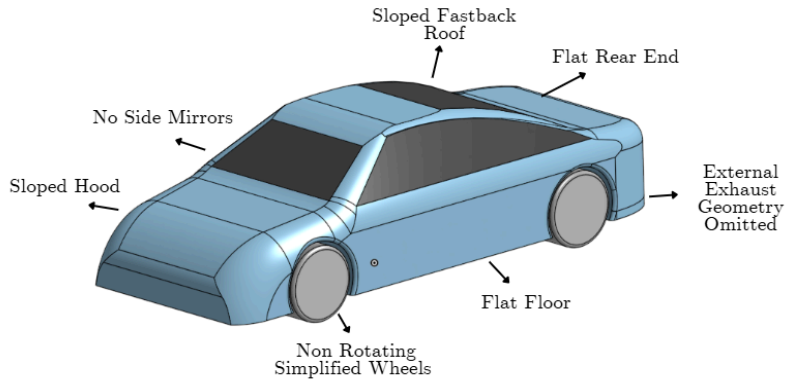
Table(6.2.8) Sources of Numerical Uncertainty

Although every effort was made to ensure numerical consistency, several sources of uncertainty remain. The simplified baseline geometry, omission of secondary vehicle features, and use of a steady-state RANS simulation introduce modelling assumptions that influence the aerodynamic coefficients obtained. Furthermore, the absence of experimental validation limits verification of the numerical predictions. Nevertheless, because all configurations were analysed using identical computational settings, the comparative aerodynamic trends observed throughout the investigation remain valid for evaluating the relative influence of progressively introduced aerodynamic devices.

7. Parametric Investigation

7.1 Configuration A (Baseline Model)

7.1.1 Render



Figure(7.1.1) labelled render of configuration A

7.1.2 Engineering Hypothesis (Configuration A - Baseline)

The simplified baseline geometry is expected to produce a large stagnation pressure region at the vehicle front, with roof-induced acceleration over the sloped fastback profile lowering local pressure and contributing to net positive lift. The flat rear end is expected to promote early flow separation, producing a low-pressure separated wake downstream of the rear body. The baseline configuration is expected to exhibit positive lift and drag dominated primarily by rear pressure separation rather than any lift-induced component, providing a suitable aerodynamic reference for subsequent configurations.

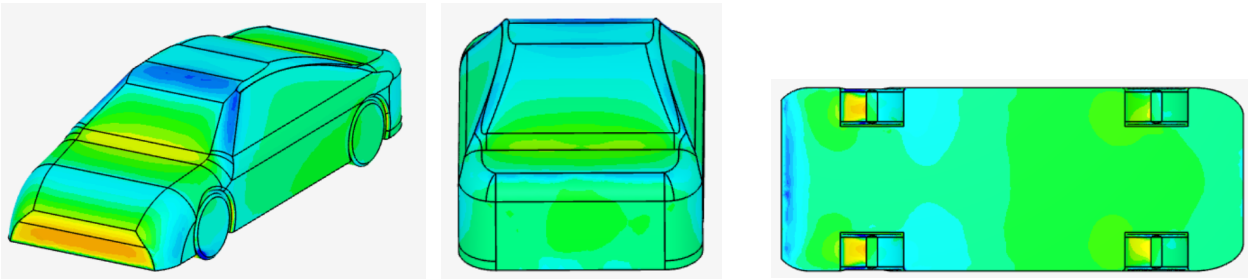
7.1.3 Quantitative Summary Table (Configuration A - Baseline)

Parameter	Value
Drag Coefficient,	0.304
Lift Coefficient,	+0.476
Front Lift Coefficient,	+0.161
Rear Lift Coefficient,	+0.310
Pitching Moment Coefficient,	−0.083

Configuration A produced a drag coefficient of CD=0.304, representing a low-drag baseline in the absence of aerodynamic devices. However, the positive lift coefficient (CL=+0.476) indicates significantly positive lift for this configuration, with the majority of the lift generated at the rear axle (CL(r)=+0.310). These results establish the aerodynamic reference against which the effectiveness of all subsequent aerodynamic modifications is evaluated.

Table(7.1.3) Aerodynamic Performance of Configuration A (Baseline)

7.1.4 Pressure Colouring

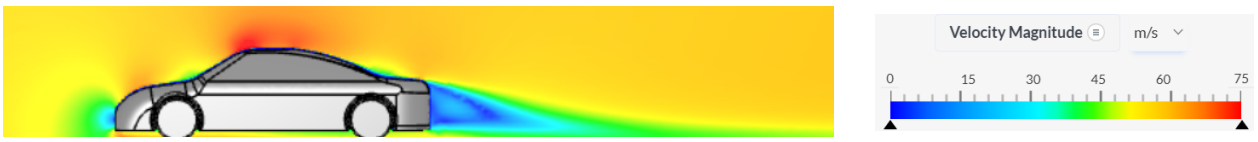


(a) Isometric **(b) Rear** **(c) Floor**

Fig(7.1.4) Showing Three views of the pressure distribution around configuration A

The pressure contours show a stagnation region at the front bumper and hood, where the incoming airflow decelerates and produces high local static pressure. Pressure decreases over the roof as the flow accelerates before partially recovering towards the rear body. The underbody exhibits relatively uniform pressure, indicating the absence of significant ground-effect acceleration in the baseline configuration. Overall, the pressure distribution is consistent with a bluff body generating positive lift and a substantial pressure wake downstream.

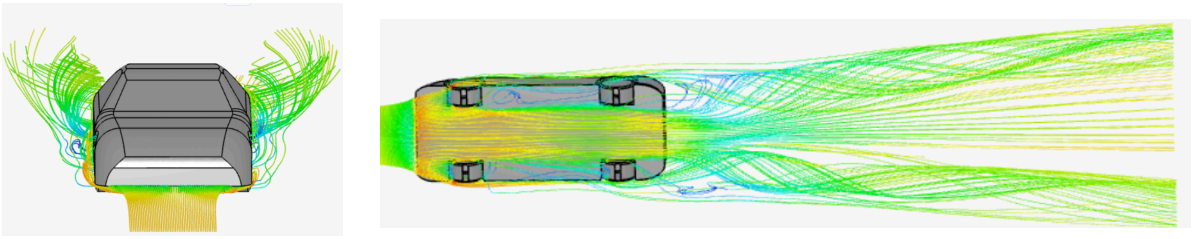
7.1.5 Cutting Plane (Velocity)



Fig(7.1.5) Cutting plane across the car showing flow velocity

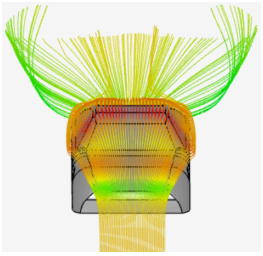
The velocity cutting plane shows flow deceleration around the front stagnation region, followed by acceleration over the sloped roof. Downstream of the rear body, the flow separates, producing a large low-velocity wake that persists several vehicle lengths behind the car. This extensive wake is indicative of significant pressure drag and is consistent with the aerodynamic behaviour expected of a bluff body baseline configuration.

7.1.6 Particle Trace Across Roof and Underbody



Fig(7.1.6(a)) Particle traces illustrating underbody flow behaviour and vortex formation in the rear wheel wake of Configuration A.

The particle traces reveal significant flow disturbance around the exposed wheels, with strong vortical structures generated by the rear wheel wake. These vortices interact with the underbody flow and contribute to the large separated wake downstream of the vehicle, indicating substantial aerodynamic losses and reduced wake stability in the baseline configuration.



The particle trace visualization illustrates a smooth flow attachment over the front body, hood and roof before separating at the rear edge, producing a broad wake downstream of the vehicle. The absence of aerodynamic flow-control devices allows the wake to expand very rapidly, contributing to the increased pressure drag and reduced aerodynamic efficiency.

Figure (7.1.6(b)) Overall Flow Development Around Hood and Upper Body of Configuration A

7.1.7 Wake Visualization using IsoVolume

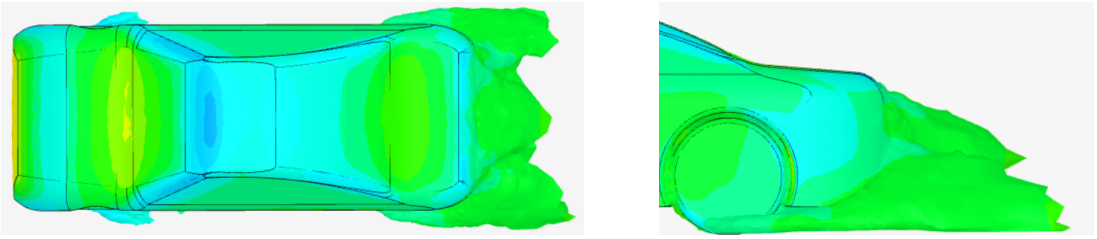


Figure (7.1.7) IsoVolume Visualization of Low-Velocity Wake (0–5 m/s) Behind Configuration A:
(A) Floor View **(B) Side View**

The IsoVolume visualization highlights the low-velocity and separated wake airflow generated downstream of the baseline car. The low-velocity zone extends about a metre behind the rear body, indicating flow separation and poor pressure recovery. Pressure colouring shows that the wake is dominated by a low-pressure region, consistent with the relatively high pressure drag observed for the baseline configuration. The zone is sloped downwards due to the high-velocity air passing down from the hood at an angle as evidenced by Fig(7.1.5).

7.1.8 Synthesis Paragraph for Configuration A

These CFD results support the given Engineering hypothesis for the Configuration A. This baseline geometry exhibits a front stagnation region, rear flow separation, and a large encompassing wake structure. The car produces a net aerodynamic lift and is a low-drag reference configuration. Therefore it provides an accurate baseline for assessing the effectiveness of subsequent aerodynamic modifications.

7.2 Configuration B (Ducktail Model)

7.2.1 Render of configuration B

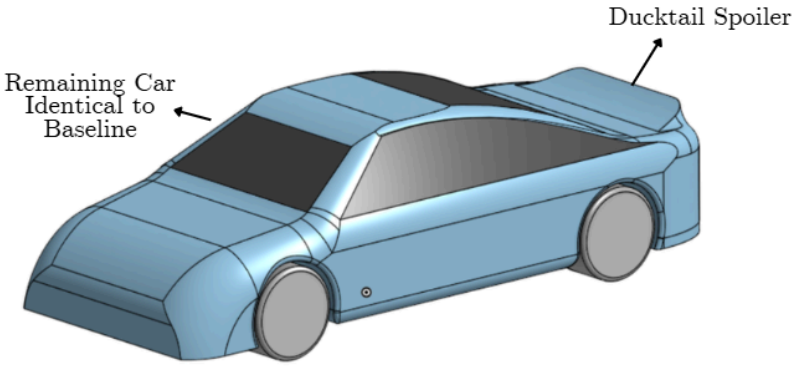


Figure 7.2 Labelled Render of the Ducktail Model

7.2.2 Engineering Hypothesis (Configuration B - Ducktail)

The airflow passing over the underbody and the sides of this configuration is expected to remain similar to the baseline car model as these regions are unchanged. However, the ducktail spoiler is expected to alter the overbody flow at the rear, increasing rear downforce and potentially reducing drag by improving wake behaviour.

7.2.3 Quantitative Summary Table (Configuration B - Ducktail)

Parameter	Value
Drag Coefficient,	0.386
Lift Coefficient,	-0.031
Front Lift Coefficient,	+0.116
Rear Lift Coefficient,	-0.147
Pitching Moment Coefficient,	+0.031

The ducktail configuration produced a final drag coefficient of 0.386 and a slightly negative overall lift coefficient of -0.031. The rear axle generated notable downforce with a lift coefficient of -0.147, while the front in positive lift coefficient of +0.116. This shows that the ducktail spoiler improved the rear aerodynamic downforce quite significantly with only a small effect on the overall pitching moment coefficient.

Table (7.2.3) Aerodynamic performance of configuration B(Ducktail)

7.2.4 Pressure Colouring (Configuration B - Ducktail)

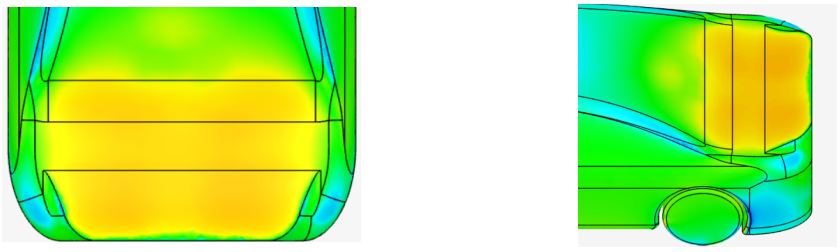


Figure (7.2.4) showing pressure colouring over the ducktail spoiler

(A) Top View **(B) Isometric View**

The pressure contours show a very clear increase in the pressure over the ducktail spoiler's surface, mostly near its central and upper regions. This indicates that the spoiler is effectively interacting with the overbody flow and modifying the rear pressure distribution, overall contributing to the observed increase in rear downforce.

7.2.5 Particle Trace (Configuration B - Ducktail)

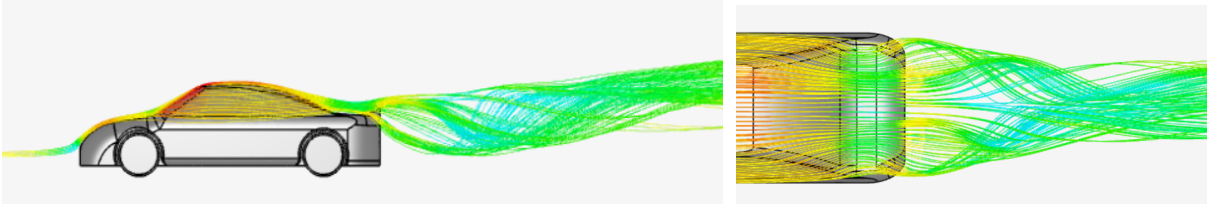


Figure (7.2.5(b)) Overall Flow Development Around Hood and Upper Body of Configuration B

(A) Side View **(B) Top View**

The particle traces show that the airflow remains attached across most of the hood and roof before being redirected by the ducktail spoiler at the rear end of the car. The spoiler alters the upper-body flow direction and wake development, producing an upward deflection of the rear flow and contributing to the increased rear aerodynamic loading.

7.2.6 Synthesis Paragraph for Configuration B

Configuration B showed that the ducktail primarily influenced the rear aerodynamic behaviour while leaving the underbody and side flow largely unchanged. The modified rear pressure distribution increased rear downforce and slightly improved the overall aerodynamic balance. Although, with a noticeable increase in drag.

7.3 Configuration C (Simple Single Element Rear Wing)

7.3.1 Render of Configuration C

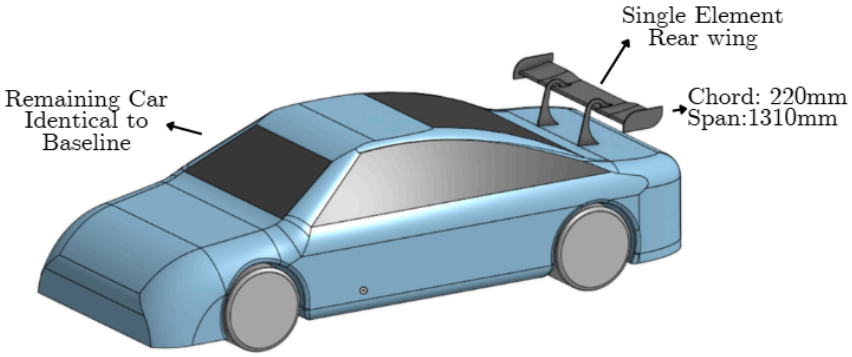


Figure 7.3 Labelled Render of the Simple Rear Wing Model

7.3.2 Engineering Hypothesis (Configuration C - Simple Rear Wing)

The single element rear wing is expected to produce an increase in the total downforce of the car by producing a pressure differential between the top and bottom surfaces of the wing. However this is also expected to be accompanied by a moderate increase in the drag of the car.

7.3.3 Quantitative Summary Table (Configuration C - Simple Rear Wing)

Parameter	Value
Drag Coefficient,	0.324
Lift Coefficient,	+0.201
Front Lift Coefficient,	+0.093
Rear Lift Coefficient,	+0.109
Pitching Moment Coefficient,	-0.008

Configuration C produced a drag coefficient of 0.324 and a lift coefficient of +0.201,which indicated that the given configuration failed to produce the expected amount of downforce. Both the front and rear lift coefficients remained positive, while the near-zero pitching moment suggests only a small change in overall aerodynamic balance. The drag penalty suffered due to the wing was marginal however.

Table (7.3.3) Aerodynamic performance of configuration C (Simple Rear Wing)

7.3.4 Pressure Colouring (Configuration C - Simple Rear Wing)

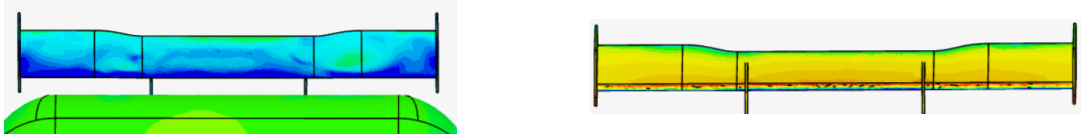


Figure (7.3.4) showing the pressure differential over the top and bottom surfaces of the wing aerofoil.

(A)Bottom View **(B) Top View**

The pressure colouring over the wing reveals an expected low pressure zone below and a high pressure zone above, generating downforce. A strong low-pressure suction zone is present right in the leading edge of the underside of the wing, which is expected due to rapid flow acceleration. However, further patchy low-pressure spots further along the underside indicate a possibility for flow separation which will be investigated further with particle trace and skin-friction colouring.

7.3.5 Particle Trace (Configuration C - Simple Rear Wing)

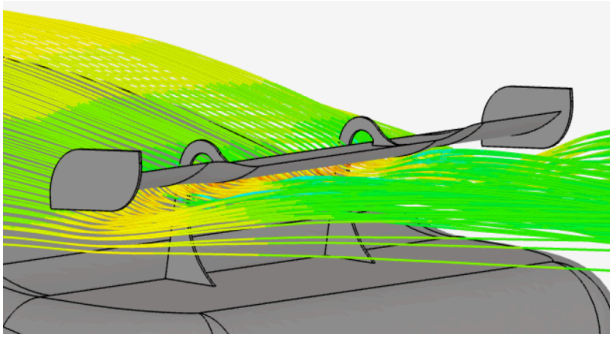


Figure (7.3.5) Showing particle trace Along the underside of the wing

The particle trace shows that the flow remains largely attached over the front portion of the wing but begins to separate closer to the trailing edge. This may be caused by an increased local angle of attack, since the incoming airflow is already directed slightly downward after passing over the vehicle roof. As a result, the wing experiences a steeper effective incidence, encouraging separation near the rear section.

7.3.6 Cutting Plane Analysis (Configuration C - Simple Rear Wing)

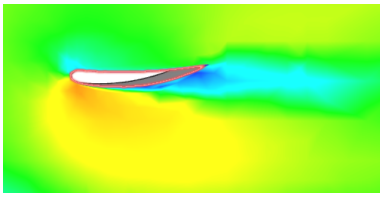


Figure (7.3.6) Showing a cutting Plane across the rear wing in the Y orientation

The velocity coloured cutting plane further supports the view of flow separation occurring in the wing by showing a distinct low velocity region near the trailing edge of the underside of the wing. This is consistent with the particle trace and the pressure colouring.

7.3.7 Synthesis Paragraph for Configuration C

The Rear wing in configuration C locally influenced the flow present in the rear of the car, it produced a local amount of downforce however was impeded by flow separation present in the trailing edge of the wing and therefore net lift was achieved for this configuration.

7.4 Configuration D (Ducktail + Rear Wing Model)

7.4.1 Render of Configuration D

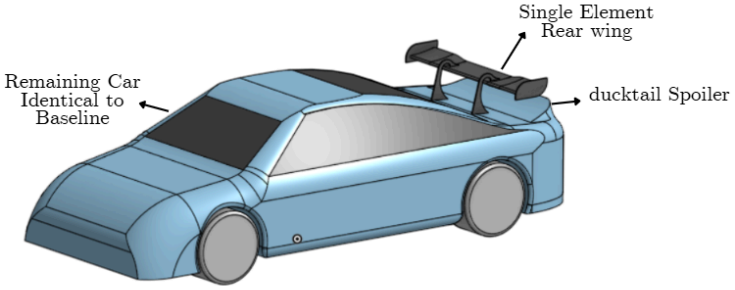


Figure 7.4.1 Labelled Render of the Ducktail+RW Model

7.4.2 Engineering Hypothesis (Configuration D - Ducktail+Rear Wing)

The proximity of the low-pressure region below the rear wing and the pressure field generated by the ducktail is expected to produce an aerodynamic interaction. This may alter the loading of both devices with the total downforce depending on whether the gain from the ducktail accelerating the airflow below the wing outweighs the loss of the high-pressure region above the ducktail leaking into the low-pressure suction zone of the wing. A slight drag increase is expected.

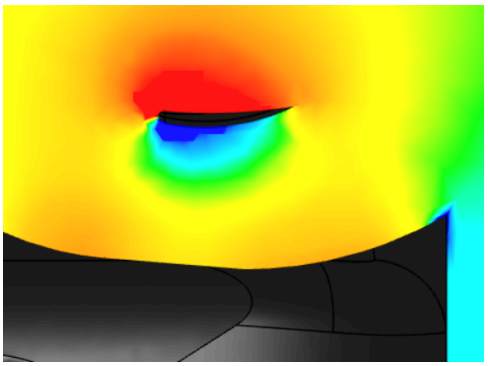
7.4.3 Quantitative Summary Table (Configuration D - Ducktail+RW)

Parameter	Value
Drag Coefficient,	0.395
Lift Coefficient,	-0.084
Front Lift Coefficient,	+0.027
Rear Lift Coefficient,	-0.111
Pitching Moment Coefficient,	-0.029

Configuration D produced a Cd of 0.395 and an overall lift coefficient of -0.084. We can see that the aerodynamic balance is shifted towards the rear axle with the majority downforce originating from there. However it is also noticed that the total downforce gained is less than the arithmetic sum of the downforce achieved individually by each element but however the drag penalty suffered is also less than the arithmetic sum of each element,

Table (7.4.3) Aerodynamic performance of configuration D (Ducktail+RW)

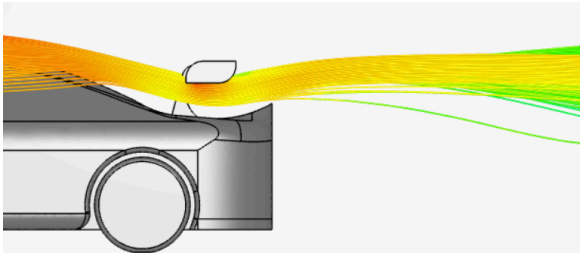
7.4.4 Cutting Plane (Configuration D - Ducktail+RW)



The cutting plane shows a clear interaction between the high-pressure region generated over the ducktail and the low-pressure suction region beneath the rear wing. Rather than remaining as a strong isolated suction zone, the underside of the wing appears to be influenced by the pressure build-up from the ducktail below it. This would reduce the pressure difference across the wing, weakening its aerodynamic loading and potentially contributing to the observed reduction in total downforce

Figure (7.4.4) Cutting plane coloured by pressure showing interaction between high and low pressure zones in configuration D (Ducktail+RW)

7.4.5 Particle Trace (Configuration D - Ducktail+RW)



The particle trace shows a clean attached flow passing through the hood and getting accelerated by the low pressure suction zone of the wing, showing that the wing actively influences the local flow despite the presence of the ducktail spoiler. These two devices primarily modify the flow passing through the rear of the car.

Figure (7.4.5) particle trace coloured by velocity in configuration D (Ducktail+RW)

7.4.6 Synthesis Paragraph for Configuration D

It was noted that the combination of the rear wing with the ducktail setup produced net downforce, the majority of which was exerted at the rear location. Visualization studies revealed that there was considerable interaction between the two setups via pressure coupling, impacting the overall effectiveness of the rear wing. Although the setup enhanced rear aerodynamic performance, such interactions restricted its total downforce capability.

7.5 Configuration E (Front Splitter+DT+RW)

7.5.1 Render of Configuration E

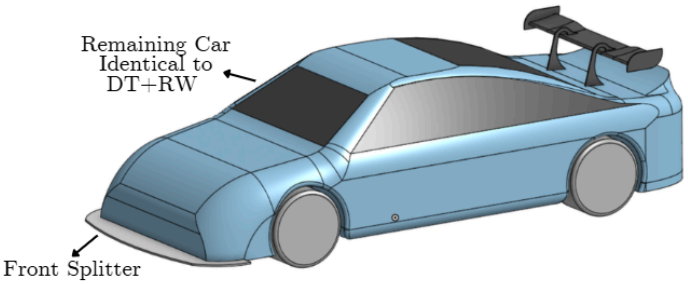


Figure 7.5.1 Labelled Render of the Front Splitter + DT+RW Model

7.5.2 Engineering Hypothesis (Configuration E - Front Splitter +DT+ Rear Wing)

The front splitter device would serve to restrict the amount of air flowing underneath the car chassis while simultaneously generating an area of high pressure above it and accelerating the flow under the chassis. As such, this should result in increased front downforce, although a minimal increment in aerodynamic drag can be anticipated because of this increased frontal area.

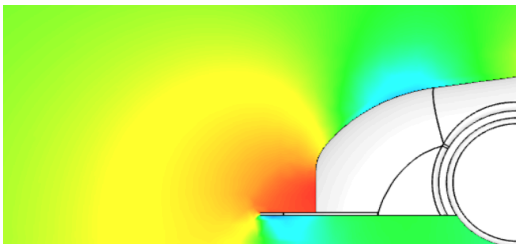
7.5.3 Quantitative Summary Table (Configuration E - Front Splitter+DT+ RW)

Parameter	Value
Drag Coefficient,	0.379
Lift Coefficient,	-0.113
Front Lift Coefficient,	-0.011
Rear Lift Coefficient,	-0.102
Pitching Moment Coefficient,	+0.044

Configuration E exhibited a drag coefficient of 0.379 alongside a lift coefficient of -0.113 for the entire body. As far as the improvement over the previous configuration goes, this upgrade focused on increasing the front aerodynamic load via modifying the front lift to -0.011 to provide slight downforce, whereas the downforce generation continued being primarily rear-based.

Table (7.5.3) Aerodynamic performance of configuration E (Front Splitter + DT + RW)

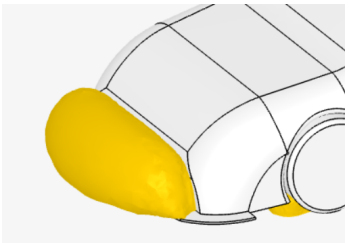
7.5.4 Cutting Plane (Configuration E - Front Splitter+DT+Rear Wing)



From analysis of a pressure cutting plane, it can be seen there is a clearly defined region of stagnation prior to the splitter, followed by regions of high-speed flow located below its leading edge. Increased velocity results in lower static pressures, contributing to front downforce created by the splitter.

Figure (7.5.4) Cutting plane coloured by pressure showing front stagnation zone caused by the front splitter in configuration E (Front Splitter+DT+RW)

7.5.5 Iso Volume (Configuration E - Front Splitter+DT+Rear Wing)



The pressure-coefficient IsoVolume highlights the high-pressure region between Cp = 0.5 and Cp = 1.5 concentrated around the front stagnation zone. This shows that the incoming airflow is strongly decelerated against the vehicle nose and splitter, therefore creating a high pressure loading which acts on the front of the car.

Figure (7.5.5) Iso Volume in the range Cp = 0.5 and Cp = 1.5 showing front high pressure zone caused by the front splitter in configuration E (Front Splitter+DT+RW)

7.5.6 Synthesis Paragraph for Configuration E

The front splitter improved the front aerodynamic loading by accelerating the underbody flow and reducing local pressure beneath the vehicle and by producing a front high pressure stagnation zone above it. This produced a small increase in front downforce while unexpectedly decreasing the total drag of the car. This drop is within the numerical noise range(3%-5%) given in section 6.2 and can hence be treated as such.

7.6 Configuration F (Simple Diffuser+FS+DT+RW)

7.6.1 Render of Configuration F

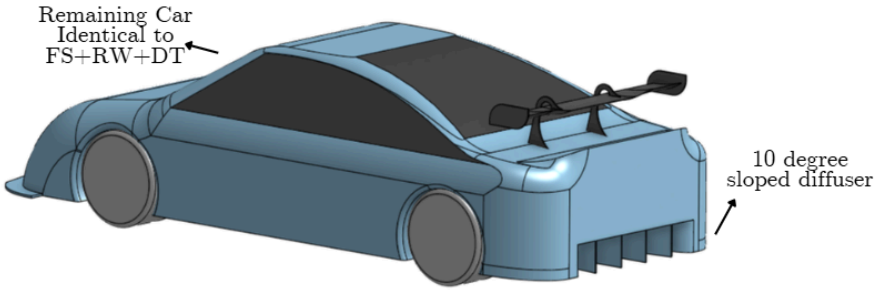


Figure 7.6.1 Labelled Render of the Diffuser+FS+ DT+RW Model

7.6.2 Engineering Hypothesis (Configuration F- Diffuser+FS+RW+DT)

The implementation of the 10-degree diffuser is expected to further facilitate the acceleration of the underbody airflow as well as its pressure recovery process towards the rear end of the car. Along with the splitter, ducktail and rear wing, this will result in greater generation of downforce, assuming that the diffuser airflow stays attached without separating.

7.6.3 Quantitative Summary Table (Configuration F - Diffuser+FS+DT+ RW)

Parameter	Value
Drag Coefficient,	0.358
Lift Coefficient,	-0.281
Front Lift Coefficient,	-0.072
Rear Lift Coefficient,	-0.209
Pitching Moment Coefficient,	+0.0031

The significant increase in downforce demonstrates that the diffuser effectively sped up the air flow in the car's underside, creating a lower pressure area underneath the vehicle. Lowering the ride height would help boost the effectiveness of the ground effect, assuming that no flow separation or diffuser choking occurred. The concurrent decrease in drag might be attributed to the improved recovery of airflow behind the car and minimization of the low-pressure recirculation bubble formed there.

Table (7.6.3) Aerodynamic performance of configuration F (Diffuser+FS+DT+RW)

7.6.4 Cutting Plane (Configuration F -Diffuser+FS+DT+RW)

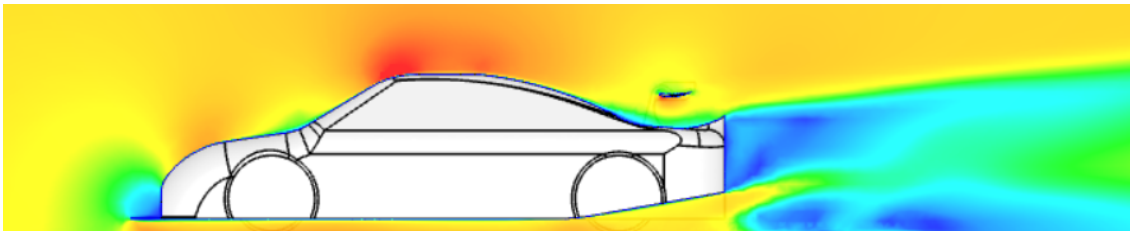


Figure (7.6.4 a) Cutting plane coloured by Velocity showing underbody flow of configuration F (Diffuser+FS+DT+RW)

The flow velocities seen on the coloured cutting plane reveal accelerated flow conditions under the vehicle approaching the diffuser, followed by flow expansion and velocity recovery towards the rear end of the vehicle. Two separation bubbles of low velocity are evident behind the diffuser. These regions indicate local flow separation and non-recovery of the wake region behind the diffuser, despite the role of the diffuser in flow acceleration and creation of downforce on the underside of the vehicle.



Figure (7.6.4 b) Cutting plane coloured by Pressure showing underbody Pressure Gradient of configuration F (Diffuser+FS+DT+RW)

The pressure cutting plane indicates a continuous zone of low pressure in the underbody region that helps in generating aerodynamic suction effects. At the rear end of the underbody, the upwardly inclined profile of the diffuser enables recovery of the pressure in order to facilitate flow expansion for attachment to the wake region. The lowest pressure is experienced right before the start of the diffuser exit.

7.6.5 Underbody Particle Trace (Configuration F -Diffuser+FS+DT+RW))

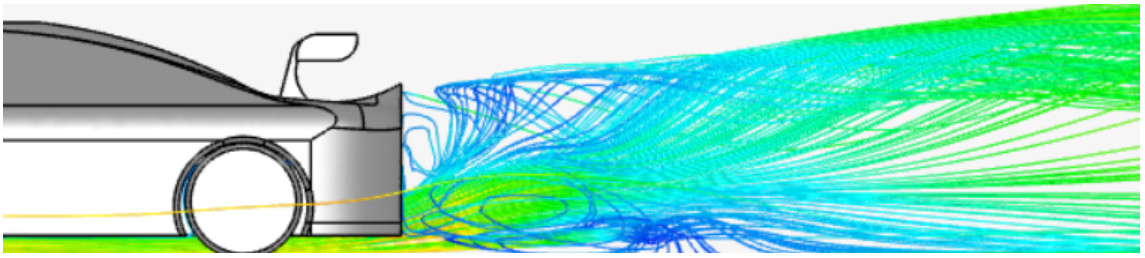
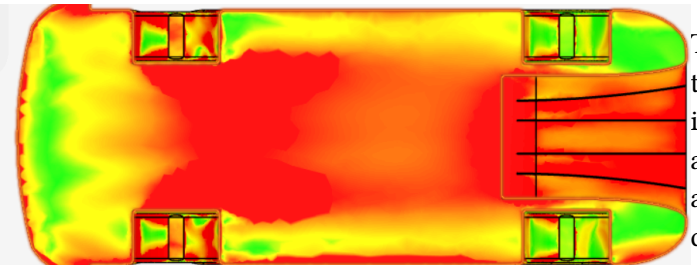


Figure (7.6.5) Particle Trace coloured by velocity showing underbody airflow of configuration F (Diffuser+FS+DT+RW)

The particle trace shows the underbody airflow being directed upward through the diffuser before entering the wake region of the car. Recirculation bubbles form immediately behind the vehicle, while the surrounding flow expands and mixes downstream. This indicates that the diffuser is recovering pressure and guiding the underbody flow, although some separation remains near the exit and downstream flow of the vehicle.

7.6.6 Wall Shear Stress Colouring (Configuration F -Diffuser+FS+DT+RW))



The wall shear stress remains high across the central floor and diffuser channels, indicating strong underbody airflow attachment. Lower values near the edges and wheel regions suggest local flow disturbance.

Figure (7.6.6) wall shear stress colouring for configuration F (Diffuser+FS+DT+RW)

7.6.7 Synthesis Paragraph for Configuration F

In summary, this design combination proved itself capable of delivering a notable enhancement in the aerodynamics of the race car through its substantial increase in downforce along with reductions in aerodynamic drag. Visualization by means of pressure distributions and flow particle tracing confirms that there was successful underbody airflow acceleration, accompanied by pressure recovery in the diffuser, although there remain recirculation areas behind the rear wheels.

7.7 Configuration G (Complex RW+Complex FS+DT+Diff+Side Skirts)

7.7.1 Render of Configuration G

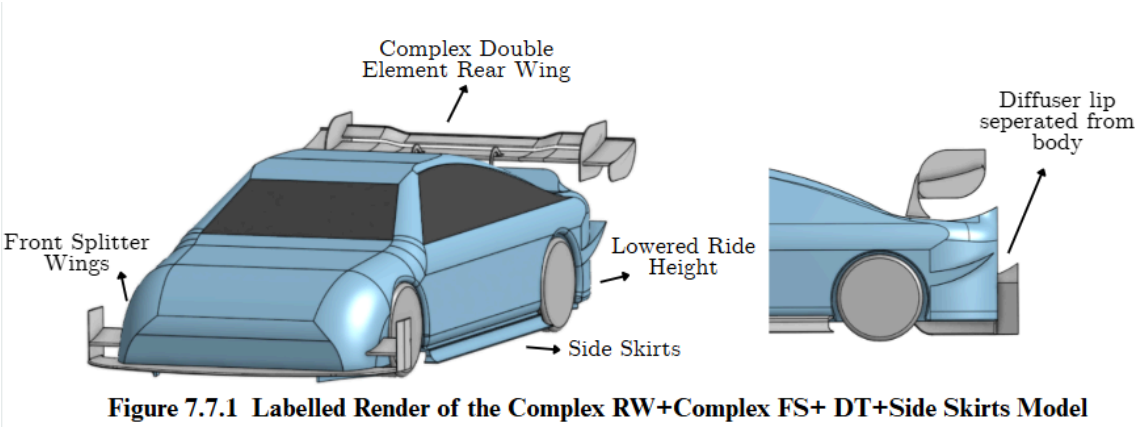


Figure 7.7.1 Labelled Render of the Complex RW+Complex FS+ DT+Side Skirts Model

7.7.2 Engineering Hypothesis (Configuration G - Complex RW+Complex FS+DT+Diff+Side Skirts)

The aerodynamic setup considered here would yield much greater levels of downforce thanks to an aggressive front splitter configuration, side-skirts, lowered ride-heights, use of a diffuser, and a double-element rear wing arrangement. The side skirts and lower ride height should strengthen underbody suction. Large aerodynamic surfaces will increase the loading of the car and will incur a high drag penalty.

7.7.3 Quantitative Summary Table (Configuration G - Complex RW+Complex FS+DT+Diff+Side Skirts)

Parameter	Value
Drag Coefficient,	0.551
Lift Coefficient,	-0.97
Front Lift Coefficient,	-0.452
Rear Lift Coefficient,	-0.520
Pitching Moment Coefficient,	+0.033

Configuration G produced a substantial increase in aerodynamic loading, achieving an overall lift coefficient of -0.97 with relatively balanced front and rear contributions of -0.452 and -0.520. This strong downforce gain came with a higher drag coefficient of 0.551, showing the expected trade-off between aerodynamic grip and efficiency.

Table (7.7.3) Aerodynamic performance of configuration G (Complex RW+Complex FS+DT+Diff+Side Skirts)

7.7.4 Pressure Colouring (Configuration G - Complex RW+Complex FS+DT+Diff+Side Skirts)

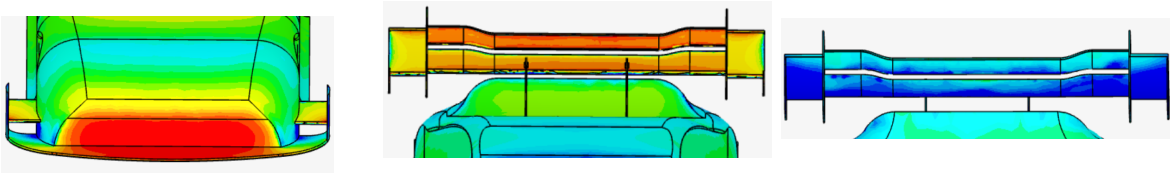


Figure (7.7.4)various views coloured by pressure of configuration G (Complex RW+Complex FS+DT+Diff+Side Skirts)

Pressure contour data reveal strong high-pressure regions present in the rear wing assembly area, coupled with sustained low-pressure areas retained below the rear wing component assembly, which results in a differential pressure capable of creating rear downforce. Similar characteristics can also be noted around the front splitter wing assembly, where the formation of high-pressure

regions takes place above the splitter wings while developing low-pressure regions underneath them.

7.7.5 Cutting Planes (Configuration G - Complex RW+Complex FS+DT+Diff+Side Skirts)

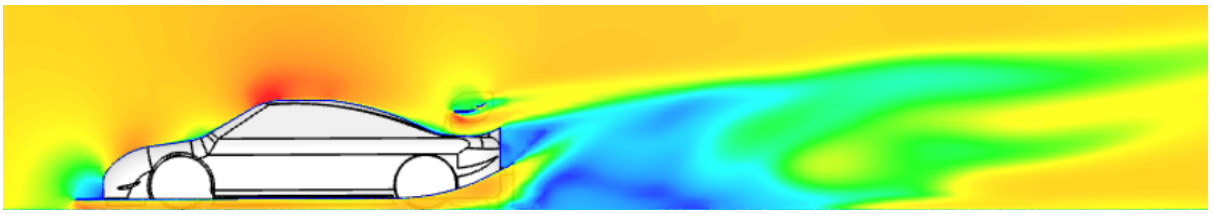


Figure (7.7.5 a) Cutting plane coloured by Velocity showing the airflow around body and larger wake structure of configuration G (Complex RW+Complex FS+DT+Diff+Side Skirts)

The velocity cutting plane demonstrates that the observed diffuser flow is consistent as being actively pulled upwards due to the low-pressure field established downstream of the rear wing, thus contributing to sustained underbody acceleration and improved recovery of pressures at the diffuser exit. The effect ensures that the rear aerodynamic configuration is treated as an integral package rather than operating separately from each other. In addition, it can be observed that the vehicle's wake is more pronounced when compared with the baseline case. This is expected, considering the additional components introduced into the vehicle's rear end ,namely, splitter, diffuser, side skirts, and multi-element rear wing, which will inevitably lead to greater flow turning and separation within the wake zone.

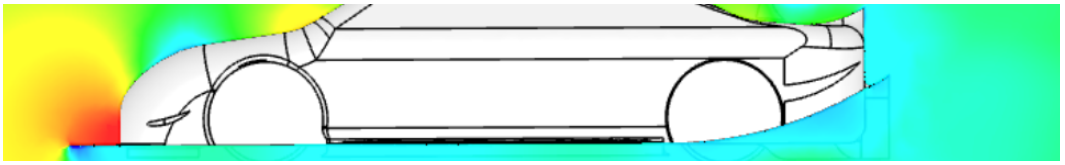
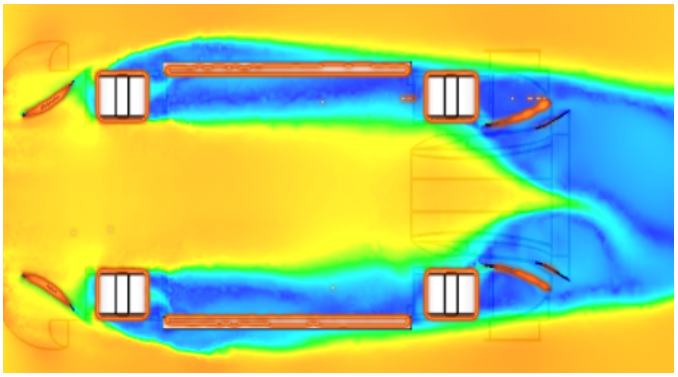


Figure (7.7.5 B) Cutting plane coloured by Pressure showing the underbody pressure gradient of configuration G (Complex RW+Complex FS+DT+Diff+Side Skirts)

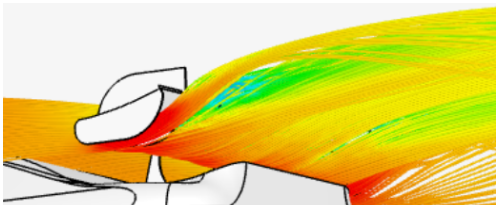
The cutting plane shows a stronger low-pressure region beneath the car, indicating increased underbody suction. This can be largely attributed to the combined efforts of side skirts along with the slightly lowered ride height,, which reduce lateral airflow leakage and help maintain a faster, lower-pressure flow under the vehicle.



Based on the findings obtained via velocity cutting plane examination, the flow emerging from the wake of the front wheel affects the flow field of the underbody before entering the diffuser region, reducing flow symmetry and limiting the effectiveness of the diffuser system. This phenomenon can be alleviated in the next iteration by implementing front wheel wake deflectors

Figure (7.7.5 C) Cutting plane coloured by Velocity showing The front wheel wake of configuration G (Complex RW+Complex FS+DT+Diff+Side Skirts)

7.7.6 Particle Traces (Configuration G - Complex RW+Complex FS+DT+Diff+Side Skirts)



Particle trace analysis reveals that the flow stays attached to both the lower and upper parts of the rear wing element. As such, it may be concluded that there is no noticeable separation occurring within the multi-element wing assembly, allowing for effective downforce generation from both parts.

Figure (7.7.6 A) particle trace coloured by velocity showing flow over the rear wing of configuration G (Complex RW+Complex FS+DT+Diff+Side Skirts)

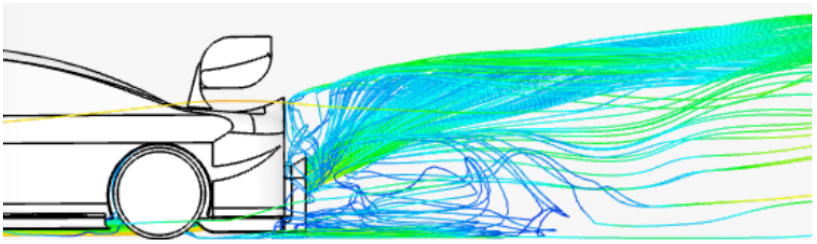


Figure (7.7.6 B) particle trace coloured by velocity showing flow across the underbody of configuration G (Complex RW+Complex FS+DT+Diff+Side Skirts)

Particle tracing analysis shows that there is considerable acceleration of the underbody flow upon entry into the diffuser channel. Following that, the flow expands and redirects towards the upward direction close to the rear end of the car. The recirculation zones present in the neighborhood of the diffuser exit are indicative of a flow disturbance. However, despite the aforementioned aspects, much of the underbody flow contains sufficient energy to allow pressure recovery within the diffuser.

7.7.7 Synthesis Paragraph for Configuration G

Configuration G achieved a major increase in overall downforce through the combined effect of the complex rear wing, splitter, diffuser, side skirts and reduced ride height. The flow remained largely attached over the wing elements, while stronger underbody suction and diffuser action improved aerodynamic loading. However, front wheel wake interference still limited diffuser efficiency and presents a clear area for further refinement.

7.8 Configuration H(Variable Height Diffuser)

7.8.1 Render of Configuration H

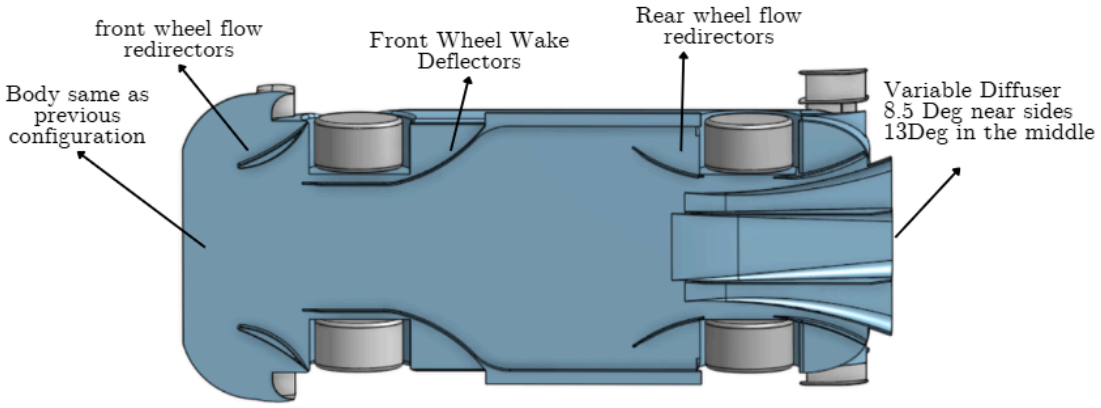


Figure 7.8.1 Labelled Render of the Variable Diffuser Model

7.8.2 Engineering Hypothesis (Configuration H - Variable Height Diffuser model)

The use of variable diffusers will be able to increase the underbody recovery of pressure through steep angles along the central portion of the diffuser, although maintaining relatively gradual angles towards the outsides in order to prevent flow separation. Additional elements including front and

rear wheel wake deflectors will serve to protect the flow under the car from any disturbance caused by the tires.

7.8.3 Quantitative Summary Table (Configuration H - Variable Height Diffuser)

Parameter	Value
Drag Coefficient,	+0.573
Lift Coefficient,	-1.452
Front Lift Coefficient,	-0.613
Rear Lift Coefficient,	-0.838
Pitching Moment Coefficient,	-0.110

In configuration H, the effectiveness of the aerodynamic loading has seen a noticeable boost with a lift coefficient of -1.452, which results from downforce that has been generated from both the front end (-0.613) and rear end (-0.838). This has taken place along with a slight increase in drag up to 0.573.

Table (7.8.3) Aerodynamic performance of configuration H(Variable Diffuser)

7.8.4 Cutting Planes (Configuration H- Variable Height Diffuser)

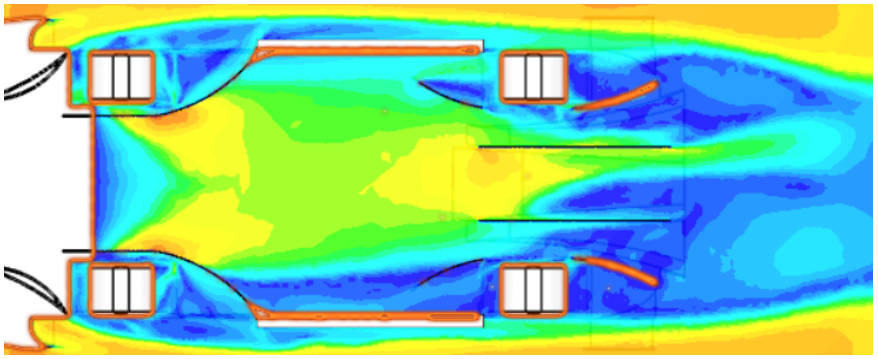
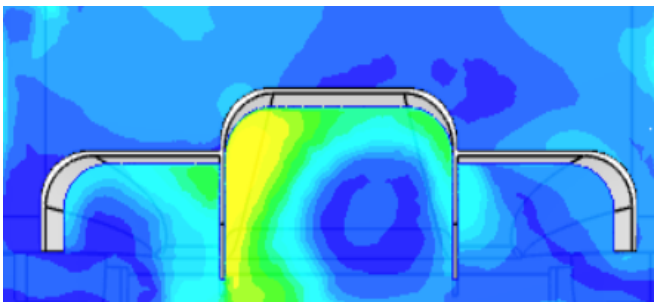


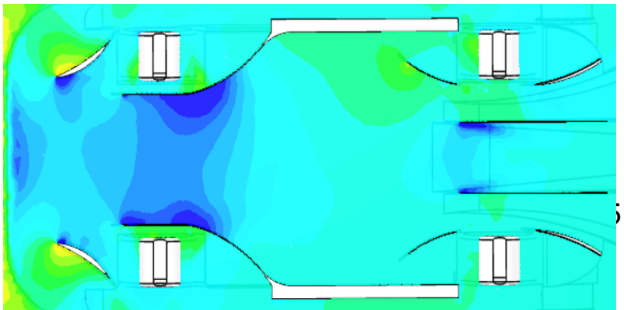
Figure (7.8.4 a) Cutting plane coloured by Velocity Showing unsymmetric front wheel wake leakage in configuration H (Variable Diffuser)

There exists a possibility that the observed asymmetrical wake state resulting from the disturbance created by the front wheel could indicate some sort of periodical/bi-stable wake flow behavior where the perturbed flow oscillates through different asymmetrical modes over time. An accurate representation would require conducting a time-dependent simulation to resolve such behavior; however, as transient simulation was out of the scope for this particular study. It should be noted that such bi-stable wake conditions have already been identified in studies of Ahmed body car flows and in real automotive aerodynamic studies[10][11].The present result is treated as a possible indication rather than a confirmed bi-stable phenomenon.



The cutting plane near the diffuser outlet exposes the presence of the turbulent wake generated from the wheel and intruding inside the right tunnel of the diffuser, the low velocity wake is also seen leaking through the central tunnel strake and entering into the central channel.

Figure (7.8.4 b) Cutting plane coloured by velocity Present near the exit of the diffuser showing wake Leaking into the right and central diffuser channel



Despite these flow inefficiencies, the underbody remains at a relatively low pressure across much of the floor. This sustained suction beneath the vehicle helps explain the high

overall downforce generated by the configuration, showing that the underbody aerodynamic system remains effective even with some local wake contamination.

Figure (7.8.4 c) Cutting plane coloured by pressure
Showing the working of the underbody of the car

7.8.5 Particle Traces (Configuration H - Variable Diffuser)

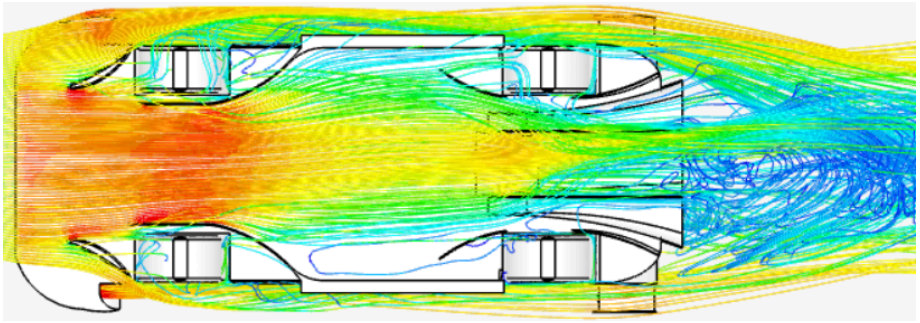


Figure (7.8.5 a) Particle trace coloured by velocity showing unsymmetric flow and flow separation in the left front wheel wake deflector

From the particle traces, it can be observed that there is asymmetry in the flow in the underbody section of the vehicle, where flow separation is taking place at the wake deflector behind the left front wheel. This causes disturbed flow and hence an asymmetric velocity distribution and pressure recovery at the bottom of the vehicle.

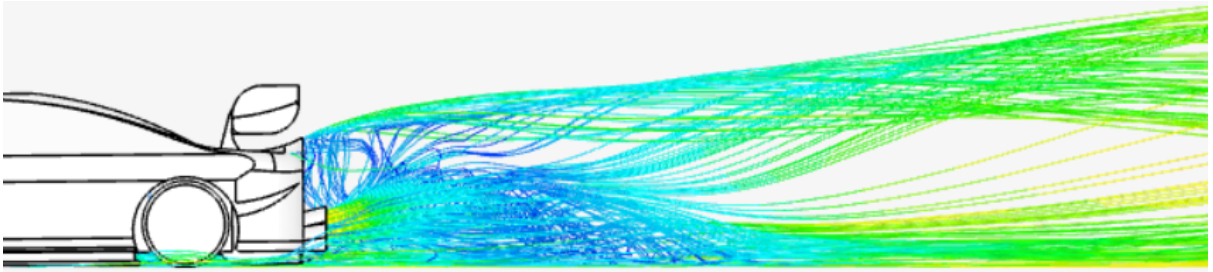


Figure (7.8.5 b) Particle trace coloured by velocity showing diffuser flow

The particle tracing analysis suggests that a certain portion of the flow exiting the diffuser enters the recirculation zone characterized by low pressure located downstream of the vehicle body. The bulk of the particles however, flow out of the diffuser smoothly without signs of any reversal flows, implying good pressure recovery despite the presence of separation and flow asymmetry

7.8.6 Synthesis Paragraph for Configuration H

Configuration H saw a significant increase in total downforce due to sustained underbody suction and improved diffuser pressure recovery. Variable diffusers and wake control aids improved aerodynamic performance; yet, asymmetrical wheel wake leakage and local recirculation persisted in reducing rear flow efficiency.

8. Comparative Parametric Analysis

8.1 Master Results Table

Config	Main Feature	Cd	Cl	Cl/Cd	Lift Improvement vs config A (%)
A	Baseline	0.304	0.476	+1.566	0
B	Ducktail Spoiler	0.386	-0.031	-0.08	106.5
C	Simple Rear Wing	0.324	0.201	+0.62	57.8
D	Ducktail + Rear Wing	0.395	-0.084	-0.213	117.6
E	Front Splitter + Ducktail + Rear Wing	0.379	-0.113	-0.298	123.7
F	Simple Diffuser + FS + DT + RW	0.358	-0.281	-0.785	159
G	Complex RW + Complex FS + DT + Diffuser + Side Skirts	0.551	-0.97	-1.76	303.8
H	Variable Diffuser + Flow Conditioners	0.573	-1.452	-2.534	405

Table 8.1: Master aerodynamic results for Configurations A–H showing CdC_d, ClC_l, aerodynamic efficiency and lift improvement relative to the baseline.

8.2 Graph 1 - (Cd vs Configuration

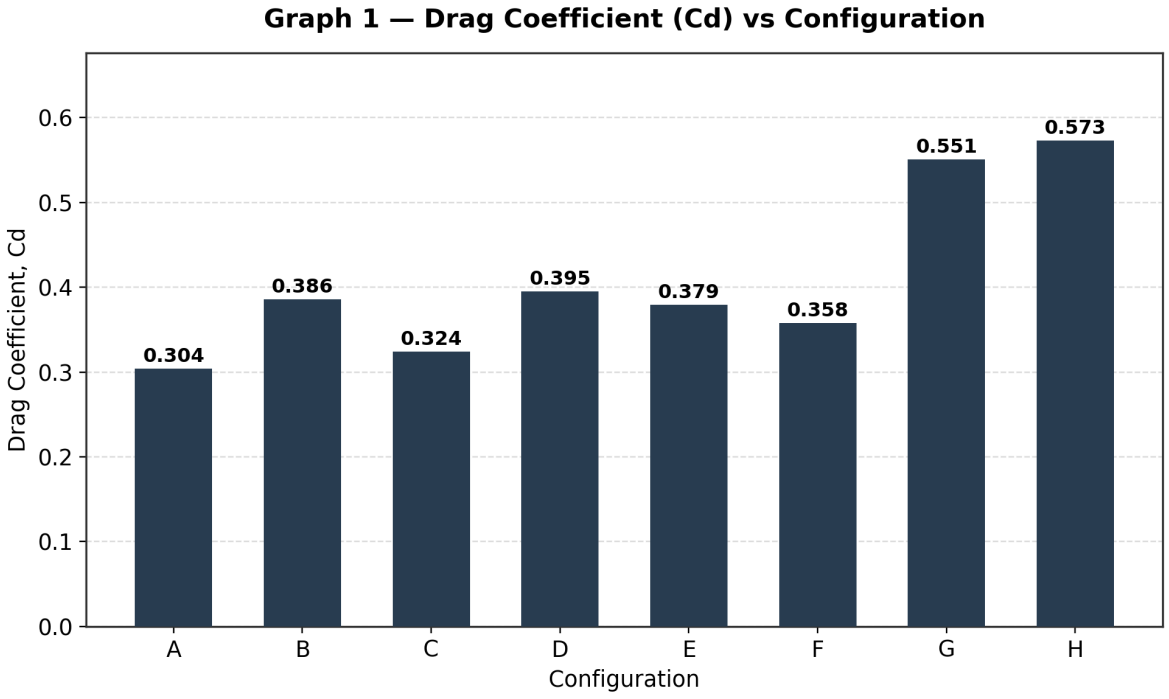


Figure 8.2: Variation of drag coefficient Cd across Configurations A–H.

8.3 Graph 2 - (CL vs Configuration)

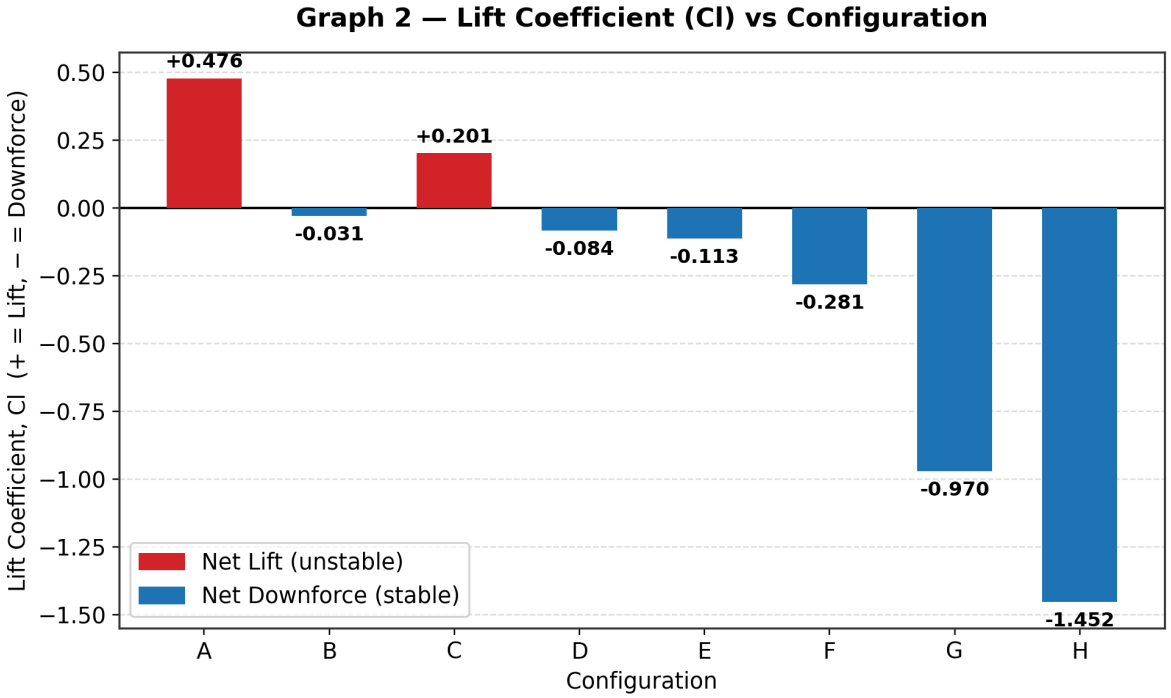


Figure 8.3: Variation of lift coefficient Cl across Configurations A–H, showing the transition from net lift to net downforce.

8.4 Graph 3 - (Cl/Cd vs Configuration)

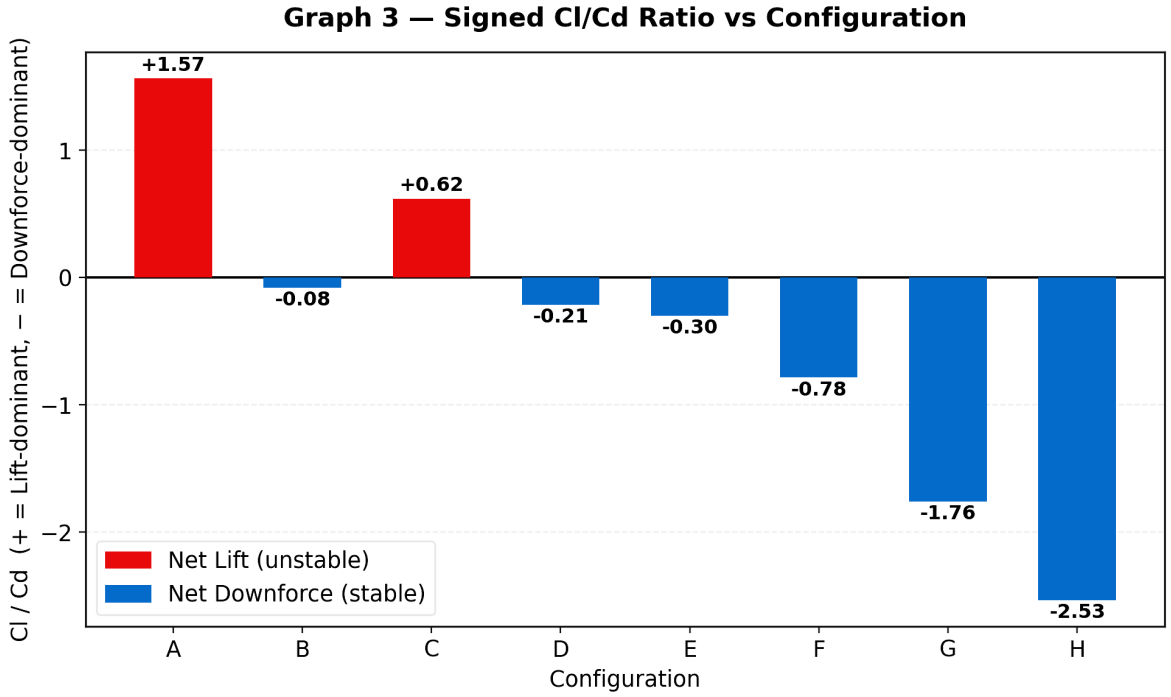


Figure 8.4: Variation of signed aerodynamic efficiency (Cl/Cd) across Configurations A–H.

8.5 Graph 4 - Aerodynamic Polar Plot (Cd vs Cl)

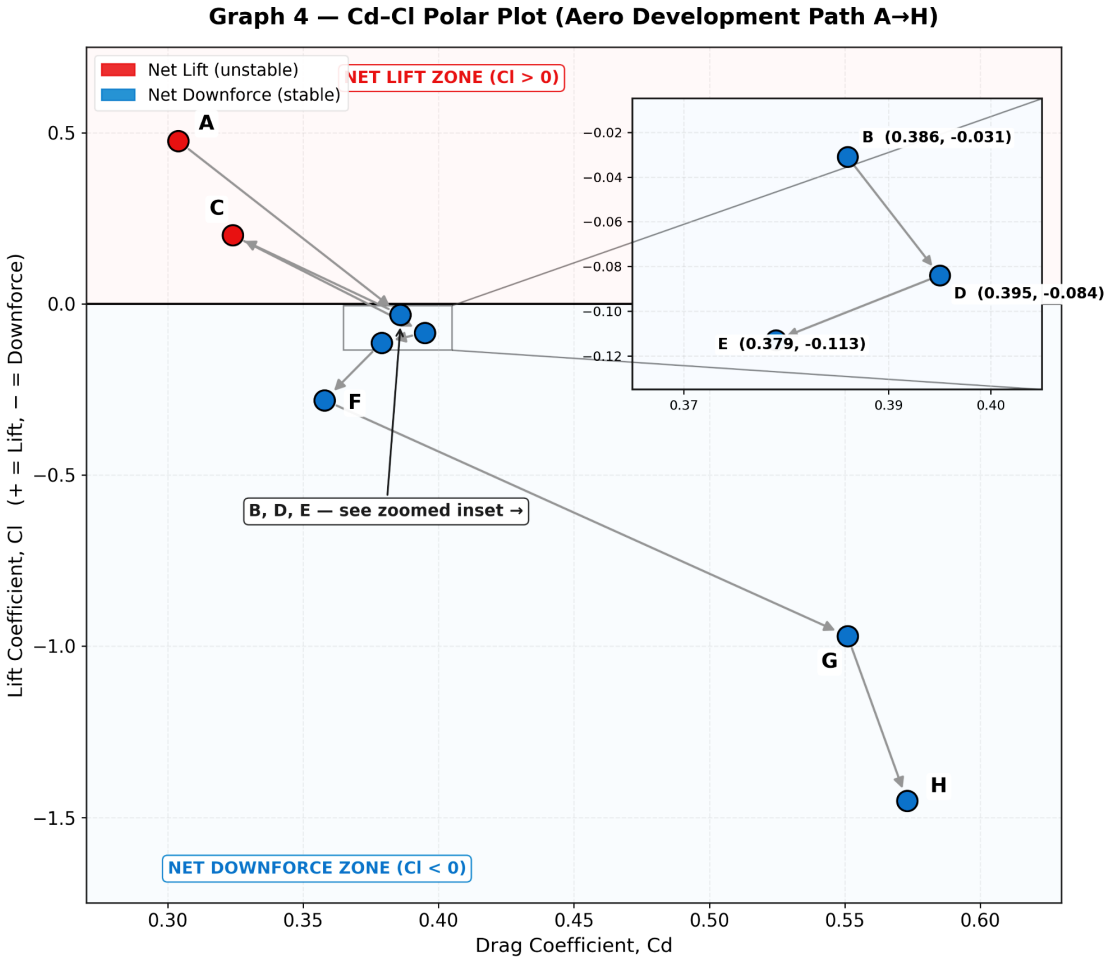


Figure 8.5: Aerodynamic polar plot showing the relationship between drag coefficient and lift coefficient throughout the A–H development sequence.

8.6 Graph 5 - Percentage Improvement (Cd & Cl)

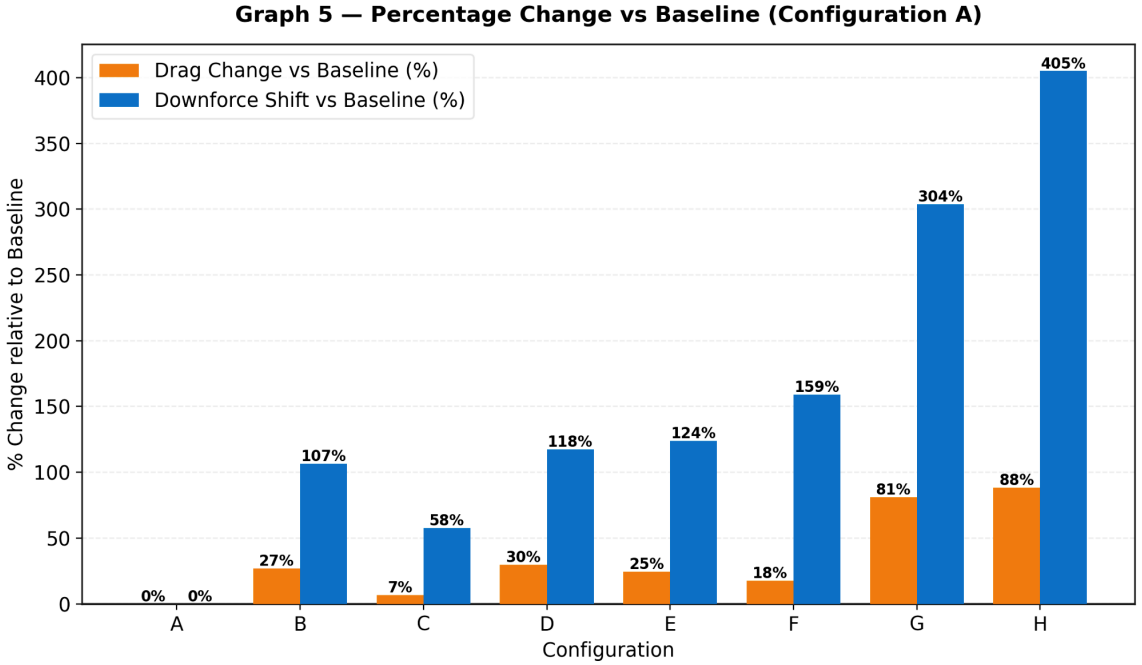


Figure 8.6: Percentage change in drag and lift performance of Configurations B–H relative to the baseline Configuration A.

9. Discussion

9.1 Aerodynamic Tradeoff

The findings reveal a clear and definite trade-off relationship between aerodynamic loading and drag with increasing complexity of the car geometry. Configuration A produced the smallest value of drag coefficient at Cd=0.304, while at the same time producing a relatively large amount of lift force indicated by Cl=+0.476. The implementation of downforce-producing components led to a gradual change towards negative values of lift coefficient. More radical designs, namely configuration G and H, were able to achieve significantly higher levels of downforce, with values of lift coefficients being Cl=-0.970 and Cl=-1.452 respectively, while also increasing drag coefficients to Cd=0.551 and Cd=0.573.

The increased value of drag may thus be explained by the greater amount of aerodynamic loading acting upon the vehicle and the higher surface area interacting with the freestream airflow. Larger wings, higher angles of attack for the wing sections, splitter surfaces, and wake energy all result in increased pressure distributions and induced drag effects. The most notable example of these phenomena occurs within Configuration G, which exhibits a significantly increased wake size due to the use of a multi-wing rear assembly, steeper splitter angle, and side skirts compared to the base configuration. On the other hand, there is no simple linear relationship between the values of drag and downforce generation. In particular, Configuration F managed to attain a large increase in downforce levels while simultaneously lowering its drag coefficient below those seen in Configuration E.

9.2 Diminishing Results

The initial hypothesis suggested that eventually the evolution of the aerodynamic systems would reach the point where any additional increase in complexity would deliver only incremental increments in the downforce generation with simultaneous increments in drag. However, the numerical findings failed to support such predictions in regard to the configuration under study. In particular, moving from Configuration D to Configuration E delivered relatively small changes in the value of the total lift coefficient, which shifted from −0.084 up to −0.113; hence implying that perhaps the aerodynamic system had reached the zone of the diminishing returns. However, adding the diffuser in Configuration F delivered much more pronounced increments in downforce generation, bringing the lift coefficient to −0.281, while simultaneously lowering the drag to 0.358.

However, the biggest gain was seen in going from configurations F to G, where the lift coefficient, Cl, jumped from -0.281 to -0.970, and similarly, the drag coefficient, Cd, also jumped up from 0.358 to 0.551. Configuration H increased the downforce to even -1.452, but with just a relatively small jump in drag to 0.573. As such, no sign of flattening out of the aerodynamic development curve was seen in the present study. The results show that further development in aerodynamics is still worthwhile at this stage. The point of diminishing return may thus be beyond Configuration H, or need even higher aerodynamic loads to be visible.

9.3 Flow Separation

Flow separation was a notable phenomenon in several designs. In Design C, there was flow separation at the tail end of the single element rear wing. Particle trace analysis and the velocity cutting plane showed that the flow did not separate over the leading section of the wing but rather detached at larger downstream positions. This is because the upstream flow had been deflected by the vehicle roof, thereby altering the incidence of the flow towards the wing. Flow separation reduced the effectiveness of the wing in producing the expected lift force.

In the case of Configuration F, there were pockets of local separation occurring just downstream of the diffuser. There were areas of low-velocity recirculation occurring just outside the diffuser discharge despite most of the flow under the car being fast and experiencing pressure recovery. The result is that the diffuser retained its efficacy, although it was not immune to the effect of separation. In Configuration G, the new multi-element rear wing had improved attachment on both wings while the diffuser still experienced disturbances due to the presence of front-wheel wakes inside the underbody.

9.4 Engineering Decision Making

From the results, it becomes clear that the development of aerodynamics is not as simple as just choosing the setup which gives the greatest downforce. The aerodynamics setup should depend on the needs of the vehicle. Setup F is important because it gives a much higher downforce compared to setups D and E. At the same time, this setup has a lower drag coefficient. Since Cd = 0.358 and Cl = -0.281, it is a relatively efficient setup in comparison to other setups where there is a compromise between aerodynamics and drag.

Constructions G and H make much more sense in situations in which aerodynamic grip is considered much more important than efficient linear speed. The considerably higher values of front and rear downforce in these configurations would be expected to help in making corners at very high speeds, but this would be achieved at the expense of greater drag and a bigger penalty to linear speed. Construction H was the most successful in terms of generating total downforce as well as Cl/Cd ratio out of all other tested constructions in this study, meaning that further development of the diffuser and airflow management proved aerodynamically valuable despite the increase in size.

One important point is that Configuration D would not be the strongest candidate for a high-speed racing circuit despite its relatively moderate complexity and aerodynamic features. Configuration F provides less drag and more downforce compared to Configuration D; therefore, it is superior from an aerodynamic perspective.

9.5 Unexpected Findings

There were several results that deviated from the original predictions and turned out to be among the most important results of the experiment. The presence of a single rear wing in the configuration C could not produce any meaningful amount of downforce on the vehicle, although there was the expected pressure difference on the surface of the wing. This can be accounted for the local trailing edge flow separation and the lack of an underwing camber to increase the low pressure suction zone

Another unexpected result was obtained during the combination of the ducktail and the rear wing in Configuration D. The resulting aerodynamic performance was not equal to the sum of both the effects of these separate elements. Due to the pressure area created on top of the ducktail and the suction area created under the rear wing, the performance was reduced. This interaction is the direct proof of aerodynamic interference between adjacent elements.

Unexpected behavior was also noticed for the underbody of the vehicle. The phenomenon of front-wheel wake interfering with the flow entering the diffuser channels was noted for Configurations G and H, thus preventing the desired pressure recovery effect and leading to an asymmetric distribution of flows inside the diffusers. This asymmetry in Configuration H could be attributed to the periodic/bistable nature of the wake, but the steady-state RANS modeling used in the present work is not able to validate such transient phenomena. Therefore, the obtained result should be treated as just an observation requiring verification by transient simulation, and not an

established aerodynamic effect. Despite these imperfections, Configuration H delivered the highest level of downforce among all configurations tested.

In conclusion, it is clear that the largest aerodynamic gains were achieved not simply by increasing the number of parts. They were rather gained by using these parts as an aerodynamic system, especially when considering the interaction between the splitter, sealed underbody, diffuser, and rear wing. At the same time, the study reveals that these interactions can be negative via phenomena like flow separation, wake contamination, or pressure coupling. The balance between these two opposite forces is one of the main conclusions of this work.

10. Conclusion

This experiment shows that gradual application of aerodynamic features can significantly improve the downforce capabilities of the car; nevertheless, the effect obtained is noticeably dampened due to the interaction of particular features. The basic configuration had minimal drag and positive lift values, whereas the further configurations gradually increased the front and rear aerodynamic forces through the use of splitter, diffuser, side skirts, and rear wing systems.

Configuration H provided the highest downforce along with the largest downforce to drag ratio with Cl = −1.452 and Cd = 0.573, whereas Configuration F had a less extreme combination with lower drag and higher downforce value. The results show that the aerodynamic performance of the car cannot be defined only by adding more devices, but depends on how efficiently the entire set manages pressure, flow under the body, and wake. The flow separation, wheel-wake interaction, and pressure coupling were still considerable drawbacks of the development.

11. Limitations and Future Work

The current research is limited due to the utilization of steady-state Reynolds-averaged Navier–Stokes (RANS) computations that fail to capture the full picture of transient aerodynamic effects. This problem becomes especially relevant when discussing the unsteady asymmetric wake found in the Configuration H, which may be indicative of the periodic or bi-stable wake dynamics. To validate such findings, transient simulations must be employed.

Another limitation can be linked to an incomplete determination of the point of aerodynamic diminishing returns. Even though some intermediate configurations have shown diminishing gains, Configurations G and H still yielded significant increases in downforce. Hence, future research should expand on the configuration matrix beyond Configuration H, utilizing more diffusers, wings, and flow conditioning until diminishing trends in downforce-to-drag ratio become clear. Transient CFD simulations and more accurate control of the wheel wake will also improve reliability of the results.

12. References

[1] R. F. Soares, A. Knowles, S. Goñalons Olives, K. Garry, and J. Holt, “On the aerodynamics of an enclosed-wheel racing car: An assessment and proposal of add-on devices for a fourth, high-performance configuration of the DrivAer model,” SAE Technical Paper 2018-01-0725, 2018, doi: 10.4271/2018-01-0725.

[2] E. N. Hogea, R. J. Hogea, and R. K. Agarwal, “3D iterative parametric optimization study of a FSAE aerodynamic package using computational fluid dynamics,” in *AIAA Science and Technology Forum and Exposition, AIAA SciTech Forum 2026*, Orlando, FL, USA, 2026, doi: 10.2514/6.2026-1898.

[3] J. Katz, *Race Car Aerodynamics: Designing for Speed*. Bentley Publishers, 1995.

[4] J. D. Anderson, *Fundamentals of Aerodynamics*, 6th ed. McGraw-Hill Education, 2017.

[5] W. H. Hucho, *Aerodynamics of Road Vehicles*, 4th ed. SAE International, 1998.

[6] F. R. Menter, “Two-equation eddy-viscosity turbulence models for engineering applications,” *AIAA Journal*, vol. 32, no. 8, pp. 1598–1605, 1994.

[7] SimScale GmbH, “K-Omega Turbulence Models,” *SimScale Documentation*. [Online]. Available: https://www.simscale.com/docs/simulation-setup/global-settings/k-omega-sst/. [Accessed: 16-Sep-2026].

[8] M. Heft, T. Indinger, and N. Adams, “Introduction of the DrivAer model: The new generic vehicle model of the Technical University of Munich,” SAE Technical Paper 2012-01-0168, 2012, doi: 10.4271/2012-01-0168.

[9] Technical University of Munich, “DrivAer: Aerodynamics of ground vehicles,” Institute of Aerodynamics and Fluid Mechanics.

[10] K. He, G. Minelli, J. Wang, T. Dong, G. Gao, and S. Krajnović, “Numerical investigation of the wake bi-stability behind a notchback Ahmed body,” *Journal of Fluid Mechanics*, vol. 926, Art. no. A36, 2021, doi: 10.1017/jfm.2021.748.

[11] G. Bonnavion, O. Cadot, A. Évrard, V. Herbert, S. Parpais, R. Vigneron, and J. Délery, “On multistabilities of real car’s wake,” *Journal of Wind Engineering and Industrial Aerodynamics*, vol. 164, pp. 22–33, 2017, doi: 10.1016/j.jweia.2017.02.004.